NASA Technical Memorandum 88798

Laser Fringe Anemometry for Aero Engine Components

Anthony J. Strazisar
Lewis Research Center
Cleveland, Ohio

Prepared for the
67th Symposium of the AGARD Propulsion and Energetics Panels
on Advanced Instrumentation for Aero Engine Components
Philadelphia, Pennsylvania, May 19-23, 1986

NASA

LASER FRINGE ANEMOMETRY FOR AERO ENGINE COMPONENTS

Anthony J. Strazisar
National Aeronautics and Space Administration
Lewis Research Center
Cleveland, Ohio 44135

ABSTRACT

Advances in flow measurement techniques in turbomachinery continue to be paced by the need to obtain detailed data for use in validating numerical predictions of the flowfield and for use in the development of empirical models for those flow features which cannot be readily modelled numerically. The use of laser anemometry in turbomachinery research has grown over the last 14 yr in response to these needs. Based on past applications and current developments, this paper reviews the key issues which are involved when considering the application of laser anemometry to the measurement of turbomachinery flowfields. Aspects of laser fringe anemometer optical design which are applicable to turbomachinery research are briefly reviewed. Application problems which are common to both laser fringe anemometry (LFA) and laser transit anemometry (LTA) such as seed particle injection, optical access to the flowfield, and measurement of rotor rotational position are covered. The efficiency of various data acquisition schemes is analyzed and issues related to data integrity and error estimation are addressed. Real-time data analysis techniques aimed at capturing flow physics in real time are discussed. Finally, data reduction and analysis techniques are discussed and illustrated using examples taken from several LFA turbomachinery applications.

INTRODUCTION

The first application of laser anemometry to the measurement of turbomachinery flow fields was reported by Wisler and Mosey in 1972 (Ref. 1). In the following 14 yr the quality and quantity of data generated by laser anemometer applications in turbomachinery has continued to increase due to advances in optics, electronics, and computer hardware. This data has been used to improve our understanding of the flow physical phenomena in turbomachinery and to validate numerical flow analysis schemes.

Until recent years laser anemometer investigations in turbomachinery have dealt with isolated rotors since flow analysis techniques have until recently been confined to the steady, axisymmetric flow regime which exists in the rotor relative reference frame for isolated rotor configurations. However, several recent experiments have involved the use of laser anemometry in studies of the periodically unsteady flow within the blade rows in single stage machines and between the blade rows in multistage machines.

The application of laser fringe anemometry to measurements in turbomachinery environments is reviewed in this paper. Example results are limited to axial-flow type compressor blading since most laser fringe anemometer experiments have involved flow surveys in fans and compressors rather than turbines. Although radial-type turbomachinery has been surveyed using laser anemometry, the majority of these applications have involved laser transit anemometry due to the generally superior ability of the LTA to make measurements in the narrow exit channels of centrifugal impellers. A recent review of published results obtained in centrifugal compressors has been given by Krain (Ref. 2). Additional LTA applications will be covered in detail in this symposium by Schodl and Elder (Refs. 3 and 4).

FUNDAMENTALS OF LASER FRINGE ANEMOMETRY

Basic Operating Principles

The operating principles of laser fringe anemometers will be briefly reviewed below. In an LFA the laser output beam is divided into two equal power beams which are focussed to a common point in space which is referred to as the measurement or probe volume. The crossing of the beams in the probe volume results in constructive and destructive interference between the train of laser light waves contained in each beam. This interference creates bright planes of light created by constructive interference separated by dark planes caused by destructive interference as shown in Fig. 1. The fringe planes are perpendicular to the plane which contains the laser beams and are parallel to the beam bisector. As shown in Fig. 1 the spacing between bright fringe planes is $s = \lambda/(2 \sin K)$. A particle which crosses the probe volume scatters light at the fringe crossing frequency, f_c. Note that the fringe crossing frequency is determined solely by the component of particle velocity U_x, which is perpendicular to the fringe planes. The U_y and U_z components carry the particle parallel to the fringe planes and do not therefore contribute to the fringe crossing frequency. Also note that while a rotation of the plane containing the laser beams about the beam bisector can be used to measure velocity components in directions between the x- and y-direction, the line of sight velocity component U_z cannot be measured.

Figure 1 illustrates three features which make laser anemometry (or LA) attractive compared to other velocity measurement techniques:

(1) The system output, i.e., the doppler or fringe-crossing frequency, is linearly related to the velocity

(2) The technique is not subject to drift since the proportionality between f_c and U_x is given by the laser light wavelength, λ, and beam crossing angle, K, both of which are constant in time

(3) The technique is only sensitive to one component of velocity

Since each of the incident laser beams is circular in cross-section, the actual probe volume shape is an ellipsoid as shown in Fig. 2. The light intensity distribution across each beam is Gaussian in shape. The beam diameter, $d_{\bar{e}^2}$, defined as the diameter at which the intensity is $1/e^2$ of the peak intensity at the center of the beam, is typically used as a measure of the beam diameter. Using this definition of beam diameter, the probe volume diameter, d_m, and length l_m defined by the $1/e^2$ intensity level can be calculated as shown in Fig. 2. Note that the ratio of probe volume length-to-diameter is given by $L/d = 1/\tan(K)$. Since the beam crossing angle K is usually between 2 and 10°, the value of L/d is on the order of 10 to 20.

Another feature of Gaussian laser beams which impacts laser anemometer optical performance is that of beam divergence which is illustrated in Fig. 3. The two important properties of the beam geometry shown in this figure are:

(1) the laser light wave front radius $R(z)$ is infinite only at the location of the beam waist, $z = 0$

(2) the output beam waist diameter $d_{\bar{e}^2}$ is related to the input beam waist diameter $D_{\bar{e}^2}$ through the formula $d_{\bar{e}^2} = 4\lambda f/\pi D_{\bar{e}^2}$.

The first beam divergence property implies that the probe volume fringes will not be parallel to one another unless the incident laser beams cross at the beam waist. If the fringe planes are not parallel, false levels of flow fluctuation will be indicated since particles of equal velocity which pass through different parts of the probe volume will generate different fringe crossing frequencies due to the variation in fringe spacing across the probe volume. A laser light collimator or mode matching lenses (see Ref. 5) can be used to insure that the beam waist will be located at the probe volume location.

The second beam divergence property shown in Fig. 3 implies that the probe volume size can be controlled through control of the incident laser beam diameter $D_{\bar{e}^2}$. Beam expanders can be used to increase the beam diameter $D_{\bar{e}^2}$, which in turn reduces the beam diameter at the probe volume, $d_{\bar{e}^2}$. From the relations shown in Figs. 2 and 3 we see that expanding the beam diameter $D_{\bar{e}^2}$ while holding the beam separation d constant results in a reduction in probe volume size and in the number of fringes in the probe volume. This results in an increase in the power density in each fringe. This in turn will result in more photons being scattered from a given particle size or in the ability to generate the same number of scattered photons from smaller size particles.

Optical Design Considerations

The successful design of an LA optical system represents a trade-off between several conflicting factors. This issue can best be addressed by considering an illustrative example.

The minimum variance which one may expect in a single velocity measurement has been shown in Ref. 6 to be

$$\sigma_m^2 = \frac{8}{\sqrt{\pi}} \frac{h.c}{\eta.\lambda.\sigma_s.\Omega} \frac{\Gamma_o}{P^2} \frac{V^3 W_o^3}{N^2 + \frac{18}{\pi^2}}$$

c velocity of light
h Planck's constant
N number of fringes
P laser power
V velocity
W_o probe volume radius
η PMT quantum efficiency
Γ_o background light flux
σ_s particle light-scattering cross-section
Ω solid angle of collection optics

This relation indicates that the measurement accuracy is enhanced by:

(1) reducing flare light and probe volume size

(2) increasing the collection optics solid angle, the laser power, and the number of fringes in the probe volume.

Flare light can be reduced by using antireflective coatings on window surfaces and by optically masking the collection optics. The solid angle of the collection optics can be increased by using large aperture (i.e., small f-number) lenses. However, the lens diameter and price increase for a given focal length as the f-number decreases and lens imperfections become harder to correct.

The probe volume size can be reduced by increasing $D_{\bar{e}^2}$ while the number of fringes in the probe volume can be increased by increasing the beam crossing angle K. However, one may reach a point at which there are not enough fringes in the probe volume or the fringe spacing is too small. Referring to Fig. 2, consider the following example: $d = 22$ mm, $D_{\bar{e}^2} = 1$ mm, $f = 200$ mm. These parameters yield a probe volume diameter of $d_m = 131$ μm containing 23 fringes with a fringe spacing of $S = 4.68$ μm. Commercially available counter-type signal processors can accurately measure fringe crossing frequencies up to 100 Mhz, but start to yield less accurate results for higher frequencies. The velocity which corresponds to a fringe crossing frequency of $f_c = 100$ Mhz is therefore a relevant parameter to consider and is equal to $V = f_c.S = 468$ M/sec for the present case. Increasing the input beam diameter $D_{\bar{e}^2}$ by a factor of 2 would reduce the probe volume diameter to 65 μm but would also reduce the number of fringes in

the probe volume to 14. This is close to the eight fringes required by most counters and can lead to angle biassing errors if Bragg shifting is not used. The number of fringes in the probe volume could be increased back to the original value of 28 by doubling the input beam spacing, d. However, this would change the fringe spacing to S = 2.35 μm and would decrease the velocity which corresponds to a fringe crossing frequency of 100 Mhz to V = 235 M/sec.

Measurement of Multiple Velocity Components

There are many optical configurations which can be constructed for measuring one, two, and three velocity components simultaneously. Reference 7 contains a rather complete description of several one-, two-, and three-component configurations as well as a comparison of the relative merits of the various configurations. This issue will be further addressed in this symposium by Boutier (Ref. 8) and will therefore be only briefly addressed below.

In turbomachinery flowfields the streamwise and circumferential components of velocity V_z and V_θ respectively, are usually much larger in magnitude than the velocity component in the hub-to-shroud direction, V_r. In addition, the radial velocity component generally lies along the optical axis of the LA system and therefore cannot be measured directly. Most LA applications to date have therefore been aimed at measuring the V_z and V_θ velocity components. Increasing emphasis on secondary flow studies is currently generating applications which require measurement of the V_r velocity component as well.

The simplest method of measuring velocity magnitude and flow angle is to acquire measurements with a one-component LA system at two different fringe orientations. Use of a one-component LA system results in two limitations. First, the statistical error in velocity, V, and flow angle, α, measured with a single-component system is greater than that resulting from a two-component system as will be described in the next section. Second, the magnitude of the turbulence components V_z' and V_θ' can only be determined if measurements are taken in the z- and θ-coordinate directions or if measurements are made at three different fringe orientations. If measurements are acquired at two arbitrary fringe orientations, one can only determine upper bounds on V_z' and V_θ'. Despite these limitations single channel LA systems have been used extensively in turbomachinery applications. The advantages of a single channel system are its simplicity and the fact that the available laser power is concentrated into a single fringe system.

Two-component LA systems can be implemented by using two colors to create two separate measurement channels. Measurement channels can also be generated by using polarization separation or by using two Bragg cells to achieve frequency separation. If signal processor logic is used to accept only those events for which a velocity measurement is simultaneously made on both channels, the statistical error in calculating V and α is reduced relative to the error obtained when using a single-component LA system and the magnitude of the turbulence components V_z', V_θ', and $V_z'V_\theta'$ will be directly measured.

Three-component LA systems can be implemented by using three colors or two colors plus frequency separation to create three measurement channels. These systems are quite complex. The accuracy with which such systems measure the radial velocity component is directly related to the off-radial beam separation angle. These systems have transmitted beams which occupy a large solid angle and which therefore require relatively large windows for optical access to the flowfield. In addition, the complex blade geometry found in most turbomachines may prevent such systems from having optical access to large areas of the flowfield.

It should be noted that one does not have to resort to a three-component LA system in order to obtain measurements of the radial velocity component. A technique in which the beams from a single channel LA system are deflected from the radial direction is described in Ref. 9. This technique uses measurements obtained from two off-radial beam orientations to calculate the radial velocity component. As will be shown in the following section, the statistical error in the radial velocity component, V_r, measured by this method will be greater than if V_r were measured directly since this technique utilizes measurements made at two different times.

A second approach to the measurement of radial velocities is reported in Ref. 10. This approach utilizes the window configuration shown in Fig. 4 to enable direct direct measurement of the radial velocity component when using the window labelled P'. While this approach does not require off-radial deflection of the transmitted beams, it can only be used in regions which are upstream and downstream of the blade row.

A third approach, which can be used to obtain radial velocity component measurements within a blade row, is illustrated in the right half of Fig. 5. The transmitted beams enter the flowpath at the blade stagger angle through an optical access hole located upstream of the blade row. Scattered light is collected in an off-axis direction through a window located over the blade row. This optical arrangement provides measurements of V_r and a combination of V_z and V_θ. The separate V_z and V_θ components are determined using the conventional approach shown on the left in Fig. 5. This approach is applicable only to a single stage machine with no inlet guide vane. Application of this approach to multistage machines would require the use of fiber optics to introduce the transmitted laser beams into the flowfield.

Statistical Measurements Errors

In order to determine accurate estimates of the mean velocity and the turbulence properties of a flow, many individual LA measurements must be acquired and averaged together. The mean and standard deviation estimated from the data are subject to both systematic and statistical uncertainty. An analysis of these uncertainties is given in Refs. 11 and 12. As shown in Ref. 11, the number of measurements required to establish a given level of confidence in the mean velocity is given by

$$\frac{V_m - V}{V} = C_v = \frac{Z}{\sqrt{N}}\left(\frac{V'}{V}\right)$$

where V is the true mean velocity, V_m is the measured mean velocity, (V'/V) is the true turbulence intensity, Z is the confidence level, and N is the number of measurements used to calculate V_m. A value of $Z = 1.97$ corresponds to a 95 percent probability that the measured mean velocity lies within the range $V(1 - C_v) < V_m < V(1 + C_v)$. The expression for the confidence level for the rms velocity estimate is

$$\frac{V'_m - V'}{V'} = C_{v'} = \frac{Z}{\sqrt{2N}}$$

where V' is the true rms velocity and V'_m is the measured value. Note that the confidence intervals are inversely proportional to $\sqrt{N}$. One therefore has to increase the number of measurements by a factor of four in order to halve the confidence interval. Also, note that C_v is proportional to the turbulence intensity, V'/V, while C'_v is independent of V'/V. Since V'/V is typically on the order of 0.1 or less, a given number of measurements always yields a much better estimate of the mean than of the rms velocity. These facts are illustrated in Table I which shows the number of measurements required to establish a confidence level of 95 percent for various values of V'/V.

An important point addressed in Refs. 11 and 12 is that the statistical error in calculating velocity components increases when using uncorrelated data acquired at different fringe orientations. Data is uncorrelated in a multichannel LA system if signal processor logic is not used to enforce simultaneity of measurements from each channel. Uncorrelated data always occurs when using a single channel LA system to acquire data at multiple fringe orientations. The magnitude of the increased statistical error can be illustrated by considering how a single channel LA system is used to determine orthogonal velocity components.

Figure 6 illustrates the calculation procedure by which velocity and flow angle are obtained with a single channel system. Measurement directions 1 and 2 shown in the figure are the directions normal to the probe volume fringes. Measured velocities V_1 and V_2, acquired at the known angles θ_1 and θ_2, are used to solve for the unknown velocity magnitude, V, and flow angle α. Orthogonal velocity components V_u and V_v can then be determined from V and α. The analysis of Ref. 11 indicates that the confidence levels in V_u and V_v are given by the expressions

$$C_u = M_u \cdot \frac{Z}{\sqrt{N}} \cdot \frac{V'}{V} \qquad C_v = M_v \cdot \frac{Z}{\sqrt{N}} \cdot \frac{V'}{V}$$

M_u and M_v are multipliers which indicate the increase in statistical error over the case in which V_1 and V_2 are acquired simultaneously, i.e., $M_1 = M_2 = 1$ when V_1 and V_2 are acquired simultaneously. If we assume isotropic turbulence, the expressions for M_u and M_v in terms of the geometry of Fig. 5 are

$$M_u = \left[\frac{\sin^2\theta_1 + \sin^2\theta_2}{\sin^2(\theta_2 - \theta_1)}\right]^{1/2} \qquad M_v = \left[\frac{\cos^2\theta_1 + \cos^2\theta_2}{\sin^2(\theta_2 - \theta_1)}\right]^{1/2}$$

Figure 7 is a plot of these multipliers as a function of the mean fringe orientation angle and the magnitude of the fringe angle difference, $\theta_2 - \theta_1$. These results indicate, for example, that for the case of $\theta_1 = 10°$, $\theta_2 = 70°$, the statistical errors in determining V_u and V_v are increased by factors of 1.217 and 1.449, respectively when using data which is not simultaneously acquired. The impact of this increased statistical error must be weighed against the increased system complexity when deciding whether to use a single or multichannel LA system in a given application.

Seed Particle Considerations

The tradeoffs between seeding the entire flowfield or using a point source of seed are briefly discussed below. In addition, the properties of a unique fluorescent seed material are described. General methods used to generate and size particles and considerations related to the particle size required to accurately follow the fluctuations in a given flowfield will be addressed in detail in this symposium by Melling (Ref. 13).

When performing laser fringe anemometer measurements in a gas it is usually necessary to introduce seed particles into the flowfield for two reasons. First, the number of particles which are naturally present in atmospheric air in the 0.5 to 1.0 μm range is generally not sufficient to yield adequate data rates. Second, by generating and injecting seed particles into the flow one can control the size distribution of the scattering particles and can therefore control to some degree the accuracy with which the seed particles follow the flow.

When designing an LA experiment one must decide whether to seed the entire flowfield (full coverage) or to seed only the stream tube which passes through the measurement volume (point injection). Both methods are used in practice and the method chosen is dependent on the particle generation rate of the seeder and on the flowfield characteristics. As an example analysis of particle generation needs, let us consider an LA application which involves flowfield measurements in the turbomachinery environment summarized below:

turbomachine diameter = 1 m
hub/tip radius ratio = 0.7

through flow velocity = 200 m/sec
volume airflow rate = 80 M^3/sec

The rate at which particles will cross the LA probe volume is given by

$$R = d \cdot L \cdot V \cdot c$$

where L and d are the probe volume length and diameter, c is the particle concentration in the flow, and V is the flow velocity.

Commercially available seeders are capable of maximum particle generation rates of 10^{11} particles/min. Coupling this rate with the volume flow rate of air through the machine yields a particle density of 2×10^7 particles/M^3 if full coverage seeding is employed. If typical probe volume dimensions of d = 100 μm, L = 1 mm are used, we arrive at a particle rate through the probe volume of

$$R = d\ L\ V\ c = (10^{-4}\ m)(10^{-3}\ m)(200\ m/sec)(2 \times 10^7/m^3) = 400\ particles/sec.$$

The actual LA data rate will be less than this number since particles which cross the probe volume outer edges usually do not scatter enough light or cross enough fringes to yield a valid velocity measurement. The conclusion to be drawn from this particular example is that point injection of seed should probably be used.

Point injection of seed is most easily accomplished through a tube placed upstream of the measurement volume as shown in Fig. 8. This tube must be placed far enough upstream to enable decay of the wake shed from the tube before the measurement point is reached. In addition, the seed injection tube is usually carried in a radial and/or circumferential actuator to enable seed injection of the stream tube which passes through the probe volume for arbitrary positions of the probe volume.

A unique seed material which has specific advantages for turbomachinery LA applications is the liquid fluorescing seed described in Ref. 14. This seed material is formed by dissolving an organic dye, rhodamine 6G, in a mixture of benzyl alcohol and ethylene glycol. When irradiated with light from the blue or green lines of an argon-ion laser, seed particles composed of this dye solution fluoresce in the orange band of the spectrum, as shown by the absorption and emission spectra shown in Fig. 9(a). By placing a narrow band orange-pass filter in the LA collection optics in front of the PMT, one can optically stop light reflected from solid surfaces at the incident light wavelength from entering the PMT. This enables one to make measurements near hub and endwall surfaces and within rotating blade rows. When not using fluorescent seed, the light reflected from solid surfaces, which is orders of magnitude higher in intensity than the light scattered by the seed particles, dominates the PMT signal as the surface is approached, i.e., the signal to noise ratio of the PMT signal drops to zero. When fluorescent seed is used, the signal to noise ratio remains constant as a solid surface is approached. In addition, since the light from the seed particles is emitted due to fluorescence rather than scattered, the Mie scattering phenomena does not apply and the intensity of light emitted by the particles is independent of direction. The penalty associated with the use of this technique is that the light-emitting efficiency of the rhodamine dye for a given size particle is generally an order of magnitude lower than the backscattering efficiency of conventional (i.e., nonfluorescing) seed particles of the same size, as shown in Fig. 9(b). In addition, both blue and green wavelengths lie in the absorption band of rhodamine as shown in Fig. 9(a). This technique therefore cannot be used with two-color LA systems.

Alternate Laser Anemometer Methods

In addition to laser fringe anemometry there are several alternate laser anemometry methods which can be used to obtain quantitative flowfield measurements in turbomachinery. These methods are Fabry-Perot interferometry; laser transit anemometry (LTA), (also referred to as the laser two focus (L2F) technique, the time-of-flight technique, and as the two-spot technique); and a hybrid method which combines features of both laser fringe and laser transit anemometers.

The LFA technique measures the frequency difference between the light scattered from each incident laser beam by a seed particle. In contrast, the Fabry-Perot technique directly measures the frequency of the scattered light by using a Fabry-Perot interferometer as a scanning optical spectrum analyzer. Development of the Fabry-Perot technique for measurements of the line-of-sight radial velocity components in a turbine cascade has been reported in Refs. 15 and 16 and will be covered in this symposium by Seasholtz (Ref. 17).

The laser transit anemometer (LTA) will be covered in detail in this symposium by Schodl (Ref. 3). The principal advantages of the LTA technique over the LFA technique are:

(1) the light intensity in the probe volume is higher than in a laser fringe anemometer which enables detection of smaller particles,

(2) the sensitive length of the measurement volume in the line-of-sight direction is much shorter than in an LFA system which enables the acquisition of measurements near solid surfaces,

(3) the LTA provides a high degree of sensitivity in flow angle measurements.

The principle disadvantage of the LTA technique is that it yields a low data rate due to the fact that the LTA measurement volume presents a much smaller "target" which a particle must hit in order to yield a velocity measurement (see Fig. 10). LTA data rates diminish rapidly as the turbulence level increases in a flowfield because the flow angle fluctuations generated by turbulence levels of 10 percent or more are large enough to prevent most particles from crossing both spots.

A hybrid technique currently under development is aimed at removing this limitation by expanding the circular LTA spots into elliptic-shaped spots. The technique represents a trade-off between power density

in the probe volume and probe volume target area. One approach to this technique is described in Ref. 18. This technique will also be discussed in this symposium by Boutier (Ref. 8).

APPLICATION OF LASER ANEMOMETRY TO MEASUREMENTS IN TURBOMACHINERY

There are three major features of the turbomachinery environment which make the application of laser anemometry more difficult in turbomachinery experiments than in external aerodynamic experiments:

(1) the close proximity of highly reflective surfaces (i.e., hub and shroud endwalls and blades),

(2) flowpath geometry (curved endwalls and complex blade shapes),

(3) the rotation of rotor blade rows.

Each of these issues will be addressed in this section. In addition, various data acquisition schemes will be compared and the advantages and limitations of each scheme will be discussed. Finally, the need to provide near real-time data reduction to support intelligent execution of experiments will be discussed.

Reflected Light Problems in Turbomachinery Applications

Two separate problems related to reflected incident light radiation arise in LFA turbomachinery applications. The first of these problems is caused by reflections from window and hub surfaces when making measurements in the flowpath inner and outer endwall regions. Reflections from the window surfaces can be reduced by using antireflection coatings on the window. Fluorescent seeding is an effective means of eliminating the problem of poor signal-to-noise ratio caused by reflection of the incident laser beams from blade and endwall surfaces.

While fluorescent seeding enables one to make measurements directly down to both the hub and shroud endwall surfaces, the proximity to a solid surface which one can achieve with nonfluorescent seeding before reflected light becomes a problem is highly dependent on the type of surface in question and on the design of the optical system. It has been the author's experience that for optical systems with beam crossing angles on the order of 5° or less employing f/4 collection optics and no special stops in the collection optics, the closest approach to a hub endwall or a window in the shroud endwall is on the order of 1 cm. For a machine with a diameter of 1 m and a hub/tip radius ratio of 0.8, a distance of 1 cm corresponds to 10 percent of the blade span.

The second source of reflected light in turbomachinery applications is "blade flash" caused by passage of the rotor blades through the incident laser beams. The severity of the blade flash problem is dependent mainly on the rotational speed of the blade row. The incident laser beams "walk" up the surface of the blade as the blade rotates through them as shown in Fig. 11. As discussed in the next section, the blades appear to be "bent" in this figure due to spanwise twist. The blade surface is in the probe volume itself for a very short time, near $t = 0$. However light can be reflected from the surface into the collection optics at any point between time $t = 0$ when the probe volume first intersects the blade surface and time $t = t_b$ when the beams are no longer blocked by the blade surface. Reflected light entering the collection optics during time $0 < t < t_b$ can cause saturation of the photomultiplier tube (PMT). If this occurs the PMT requires a finite amount of time to recover and measurements which occur during the recovery time will be lost. For rotors operating at tip speeds on the order of 400 to 500 m/sec, blade passing frequencies are on the order of 5 to 15 Khz, and time t_b is on the order of 7 to 20 μsec. However for low speed machines this time can be at least an order of magnitude greater. It has been the author's experience that reflected light from blade surfaces does not cause PMT saturation in high speed machines but can cause problems in low speed applications. Fluorescent seeding therefore appears to be necessary in high speed applications only when measurements in the proximity of the hub or shroud endwalls are desired.

Blade Geometry

One feature of turbomachinery geometry which impacts optical access to the flowfield is spanwise twist of the blading as shown in Fig. 12. This twist leads to the "bent" appearance of hub-to-tip blade sections such as AA and BB when viewed in a streamwise direction. For blades which are radially stacked about the c.g. of each section this bending is worst near the leading and trailing edges. If the incident laser beams are constrained to enter the flowpath in the radial direction, shadowed regions occur as shown in which the tip blade section prevents optical access to the hub section. The extent of the shadowed region can be as great as 20 to 30 percent of the blade pitch at the hub. This shadowing can be eliminated if the LA optical system is capable of orienting the incident laser beams away from the radial direction as shown in Fig. 12.

When acquiring measurements at design speed operating conditions, use of the blade design geometry is generally an accurate method of calculating the information required to relate the axial and circumferential measurement location to the blade surface location. However, at part speed conditions the blade geometry will vary from the design geometry due to deflections caused by reduced mechanical stresses. The principal deflection in axial-type blading is an untwist or change in the blade stagger angle as shown schematically in Fig. 13(a). The amount of untwist varies from zero at the hub to a maximum at the tip. Axial blading also experiences some axial deflection due to thrust loading. In radial-type blading the primary deflection due to mechanical stress is a "flowering" of the rotor disk, which causes a shift in the axial location near the rotor exit. These deflections can be accounted for by measuring the actual location of the rotor during data acquisition and correcting the design blade geometry as required.

The blade geometry at the tip can be measured during data acquisition by positioning the probe volume at the tip radius. If seed injection is turned off, the fringes are oriented to measure the circumferential velocity component, and the laser power is reduced, then the LA signal processor will perceive the

blades passing through the probe volume as seed particles. Since velocity measurements will only occur over the blade tip, the blade circumferential location can be determined from the location at which measurements have occurred. The sensitivity of such a procedure to changes in the blade stagger angle can be controlled by the circumferential resolution of the LA measurements. Results obtained from an axial-flow fan using the above procedure are presented in Fig. 13(b). As described in Ref. 19 the measurements were acquired in a 51.3 cm diameter rotor using a resolution of 1000 measurement locations per blade pitch. The rotor has 22 blades which yields a circumferential resolution of 0.008 mm. The measured untwist was 1.96±0.04° compared to a finite element analysis prediction of 2.02°. These measurements also indicated that the blade spacing around the wheel was uniform to within 2 percent.

Window Design Considerations

Optical access to wind tunnel models used in external aerodynamics experiments is usually provided through flat windows mounted in the tunnel walls. The use of flat windows in turbomachinery applications leads to distortions in the outer flowpath due to shroud curvature in both the circumferential and streamwise directions, as shown in Fig. 14 for an axial-type blade. This flowpath distortion is often greatest in the rotor tip region and can significantly alter the local tip clearance. This problem is particularly acute in radial turbomachinery applications, where the shroud radius of curvature is small in both the circumferential and the streamwise direction.

Flat windows are required for laser transit anemometer applications, since the highly focussed "spots" of a transit anemometer become highly defocussed if the window is not flat. This defocussing reduces the power density in each spot to levels which are unuseable. Flat windows are not required for laser fringe anemometers.

One solution to the need for flat windows in curved flowpaths is the use of many small windows, as shown at stations 5 to 14 in Fig. 15. Such an approach is the only one practical for radial-type turbomachines if one desires to maintain proper tip clearances or to use laser transit anemometry. However, as seen in Fig. 15, the use of many small flat windows limits one's ability to acquire measurements at arbitrary streamwise locations.

For axial-flow configurations, in which streamwise radii of curvatures are relatively large, curved windows can be easily fabricated by heating flat glass plates to the yield temperature of the glass and forming the glass over a mold. Such windows follow both the circumferential and streamwise curvature of the flowpath and offer unlimited access to arbitrary axial and circumferential measurement points within the window boundary.

Refraction at the air-glass interface on window inner and outer surfaces causes the following phenomena which impact measurement accuracy:

(1) The actual probe volume location is translated relative to the location which would have occurred without refraction effects,

(2) The incident laser beams which generate the probe volume may uncross - i.e., the two beams will no longer lie in the same plane,

(3) The beam crossing angle, which affects the calibration factor between fringe crossing frequency and seed particle velocity may change.

Probe volume translation will always occur for both flat and curved windows, while changes in beam crossing angle only occur for curved windows. Beam uncrossing occurs when the solid angle between the incident laser beam and the window surface is not equal for each beam in a fringe anemometer. Beam uncrossing thus generally occurs for curved windows but can occur for flat windows when the beam bisector is not perpendicular to the window surface. If the uncrossing distance at the probe volume location is comparable to the beam diameter, the beams will no longer intersect one another and the probe volume will be destroyed. A change in beam crossing angle can occur only across a curved window. The crossing angle changes when the change in surface normal orientations between the window outer and inner surfaces are not the same for both laser beams.

The magnitude of window refraction effects is dependent on the beam crossing angle, the probe volume immersion into the flow, the window thickness and radius of curvature, and the orientation of the incident laser beams relative to the window. These effects have been recently studied in detail for flat and cylindrical windows using an optical ray tracing technique which is applicable to totally general window shapes (Ref. 20). The impact of typical values of these parameters on the uncrossing problem is shown in Table II. The conclusion which one draws from this example is that relatively thin windows are required when curved windows are used. We generally use a window thickness of 3 mm in our research rigs, which have a diameter of 0.51 m.

One very promising solution to the uncrossing problem is presented in Ref. 21. The procedure involves making an interference hologram between a reference beam and a laser beam which passes through the window after passing through the desired measurement point as shown in Fig. 16. The hologram can then be used to introduce an exact refraction-error correction into an incident laser beam which follows the path of the reference beam used to create the hologram. The hologram deflects the beam onto the path required to pass through the window and the measurement point. The technique is suitable for high laser power levels (on the order of 2 W) due to the high transmission efficiency of the hologram. The only disadvantage of this technique is the need to make a hologram for each different location at which one wishes to pass through the window.

Window Cleaning

The use of seed injection into the flowfield in order to enable LA measurements can result in the accumulation of seed particles on window inner surfaces. This deposition is due to large particles which

do not follow the flow and are therefore centrifuged out toward the shroud. In addition, turbomachinery component research rigs usually have lower quality oil seals than flight-certified engines, which can cause window contamination due to oil leakage even when seed material is not used. An effective method of removing deposits from windows is the injection of a liquid solvent into the flow through small holes located in the shroud upstream of the window. Window cleaning by this method is especially effective in the region over the rotor tip, where the liquid is scraped across the window by the rotating blades. The author has been able to wash windows in single-stage axial compressor applications for rotors with tip speeds on the order of 425 m/sec without reducing the rotor speed, which allows the operating point to remain unchanged during window washing. The use of liquids for on-line window washing may not be practical for applications in higher pressure ratio centrifugal compressors and multistage axial compressors. In such machines the flowfield temperature rise may be so high that window washing liquids would evaporate or cause high thermal stresses when they coat a hot window.

Measurement of Blade Rotational Position

A laser anemometer measurement is a random event triggered by the presence of a seed particle in the probe volume. When acquiring measurements in rotating blade rows one must therefore measure the blade row rotational position every time a velocity measurement occurs. There are four measurement methods which can be used to provide this rotational position:

(1) Enable a measurement window once-per-rotor revolution during data acquisition.

(2) Enable a measurement window once-per-blade passing during data acquisition.

(3) Enable continuous measurement windows during data acquisition.

(4) Record the time between measurements and assign measurement windows after data acquisition.

Methods (1), (3), and (4) require a once-per-rev (OPR) timing signal from the rotor while method (2) requires a once-per-blade (OPB) timing signal.

The generation of measurement windows for the first three methods is shown schematically in Fig. 17. By definition a measurement window is a time interval used to classify velocity measurements according to the rotational position at which they occurred. All velocity measurements which occur within a given window are spatially averaged across the width of the window. It is therefore advantageous to keep the measurement windows narrow. Since LA measurements are usually displayed graphically as discrete measurement points across the blade pitch, it is important to remember that each point represents a spatial average across the window width.

Implementation of methods (2) and (3) for generating measurement windows requires the ability to subdivide the time between once-per-blade (OPB) and once-per-rev (OPR) signals respectively. This requirement is met by generating pulse trains at frequencies which are integral multiples of the OPB or OPR signal frequencies. These pulses are accumulated in a counter which is initialized by each OPB or OPR signal. Whenever an LA velocity measurement occurs, the current counter contents are recorded with the LA measurement as a (velocity, clock count) data word pair. The clock count is then used to determine the measurement window in which the velocity measurement occurred.

Note that a variable delay after the once-per-rev signal is needed in order to align the measurement windows with the blade passage. This effect is illustrated in Fig. 17 by delays D_1 and D_2 which are required for measurement axial locations ZM_1 and ZM_2, respectively. Successful implementation of methods (2) and (3) also requires the use of fairly high frequency pulse generators, as shown in the table below for two typical high speed compressor applications.

FREQUENCY REQUIREMENTS FOR WINDOW-GENERATING PULSE TRAIN

[NB - number of rotor blades; BPF - blade passing frequency; NWP - number of windows per blade passage; F - pulse train frequency; WW - window width in microseconds]

Machine type	rpm	NB	BPF, Khz	NWP	F, Khz	WW
Centrifugal						
Main blade	36 000	20	12	16	192	5.2
Main and splitter blade		40	24	16	384	2.6
Axial	20 000	40	13.3	50	665	1.5

Use of constant frequency pulse generators will result in changes in the number of measurement windows between OPB or OPR signals due to rotor speed variations. One must therefore use a phase-locked loop or a tracking shaft angle encoder (Ref. 22) which is capable of rapidly varying the pulse generation frequency in response to rotor speed variations. For high speed applications a digital shaft angle encoder is preferred over a phase-locked loop, since the response lag in phase-locked loops is generally too large to enable accurate tracking of rev-to-rev variations in rotor speed.

The first method listed above is the simplest, and involves enabling a measurement window after a known time delay τ has elapsed after occurrence of the OPR signal. A blade-to-blade velocity profile can be achieved by collecting measurements for various delay times τ. This method allows one to obtain measurements in different blade passages around the wheel. It is the simplest of the four methods and was

therefore used in early applications of LA to turbomachinery (see Ref. 23 for example). While it is simple to implement this method is also inefficient since the measurement window is only opened once per rotor revolution.

In method (2) a fixed number of measurement windows are generated between adjacent once-per-blade (OPB) signals. Since the OPB signals from each blade are all identical, measurements which occur within a measurement window can come from any blade passage on the wheel. This method is more efficient than method (1) since it opens a measurement window at all times. However, in order to measure the flowfield in an individual blade passage, the windows must be enabled for only the passage of interest. In this case data can only be acquired during a time corresponding to (1/NB) of each revolution, where NB is the number of blades. Reference 24 describes the use of this method in a laser transit anemometer system.

Method (3) essentially opens measurement windows at all times and assigns a unique set of measurement windows to each blade passage. This technique therefore allows maximum data acquisition efficiency when one is interested in obtaining measurements in individual blade passages. Use of this technique in a laser fringe anemometer system is described in Ref. 22.

The fourth data acquisition method is similar to the method (3) in that it assigns a unique set of measurement windows to each blade passage. This method, which is described in Ref. 25 for a two-bladed propeller, is shown schematically in Fig. 18. During data acquisition, a trigger signal is recorded once-per-rev along with the elapsed time between each LA measurement. The pitchwise location of each measurement is then determined after data acquisition is complete by using the time-between-measurement data and the triggering pulse (or OPR) data. After the pitchwise measurement location is determined, the measurement is assigned to the appropriate window. Since measurement windows are defined by the user during post-run data processing, this method allows the user the freedom of changing the width and number of the measurement windows without rerunning the experiment. In contrast to methods (1) to (3), this method also enables the user to determine the circumferential location of each LA measurement within the measurement window. This information can be used to assess the degree of spatial averaging which occurs when all measurements within a window are averaged together.

The four approaches discussed above are by no means the only methods which can be used to determine the blade row rotational position for each LA measurement. An approach which is a hybrid of the third and fourth approaches discussed above is described in Ref. 26. This method is similar to method (4) in that it determines the rotational position from the time-between-measurements and a triggering pulse. However, in this method the triggering pulses are generated by an encoder which generates up to 1000 pulses/rev (similar to method (3)), while in method (4) the triggering pulses are generated once-per-rev.

Data Acquisition Methods

The various methods of recording rotational position discussed above allow one to implement several different data acquisition methods. The method which one chooses to use is dependent on the level of information which one is trying to extract from the measured flowfield and on the level of flowfield periodicity.

Averaging Methods

The simplest data acquisition method which enables one to determine the blade-to-blade distribution of velocity and flow angle within a rotating blade row can be referred to as a "blade average" mode of data acquisition. This data acquisition method can be implemented using method (2) discussed above for recording the blade rotational position. When performing blade average data acquisition one generates measurement windows between successive once-per-blade signals. Measurements which are assigned to a given measurement window can originate from any blade passage around the rotor. When using this method one is therefore averaging together the flowfields which occur in each individual passage, and all information concerning passage-to-passage flowfield variations is lost.

A second, more complex method of acquiring data can be referred to as a "window average" mode of data acquisition. This method can be implemented using method (3) discussed above for recording the blade rotational position. All measurements which occur within a measurement window are known to originate from the particular blade passage in which the window lies. Window-average data acquisition therefore allows measurement of the blade-to-blade distribution of velocity and flow angle in individual blade passages, which in turn allows one to assess the level of passage-to-passage flowfield variations around the rotor. Although window average data acquisition provides more information than blade average methods, information concerning the distribution of the individual velocity measurements which occur within a measurement window is still lost during data acquisition. Blade and window averaging methods average together all measurements which occur within a given measurement window. As shown in Ref. 9, if one records the number of measurements, N, which occur within each window, the sum of the measured velocities, ΣV_i, $i = 1, N$, and the sum of the squares of the measured velocities, $\Sigma(V_i)^2$, then one can calculate the mean and standard deviation of the measurements which occurred within the window using the following:

$$\bar{V} = \sum_{i=1}^{N} \frac{V_i}{N}$$

$$V' = \left[\sum_{i=1}^{N} \frac{\left(\bar{V} - V_i\right)^2}{(N-1)} \right]^{1/2} = \left[\frac{\left(\sum_{i=1}^{N} V_i^2 - N\bar{V}^2 \right)}{(N-1)} \right]^{1/2}$$

Note that only five words of information, N, ΣV, ΣV^2, need to be recorded for each measurement window (one word for N which is an integer and two words each for ΣV and ΣV^2 which are real numbers).

In addition, the number of words stored is independent of the total number of measurements acquired during a run.

As shown in Refs. 9 and 22, the window average mode of data acquisition can be an efficient method of obtaining good blade-to-blade spatial resolution while minimizing computer storage requirements. The LA system described in these references generates 50 measurement windows across 20 consecutive blade passages. The system therefore records velocity measurements in 1000 measurement windows while using only 5000 words of computer storage. As discussed in Ref. 22 and shown in Fig. 19, the window number (referred to as "shaft position" in Ref. 22) is used as an address in a stored data array. This scheme enables efficient real-time processing and graphical display of the measured data because the data is assigned its proper place in the data array as part of the measurement process.

Data Capture Method

The most complete method of data acquisition can be referred to as a "data capture" method. In the data capture method, each individual velocity measurement which occurs within a window is individually recorded, and the velocities are not summed during data acquisition. This data acquisition mode therefore allows the user to examine the probability density distribution of the measurements which occurred within each window.

There are several advantages and disadvantages to be considered when deciding which data acquisition mode to implement. The data capture method lends itself to direct memory access (DMA) transfer of data from LA counter processors to computer core memory since all measurements are recorded without any averaging or summing. However, this method can require large amounts of computer core memory and archival storage relative to the blade and window average methods since two words of information (integer representation of measured velocity, window number) must be recorded for each measurement.

Consider for example a situation in which one wishes to record velocity measurements in 25 windows from blade-to-blade across 40 individual blade passages. In addition, assume that one wishes to record 100 measurements in each window and that the data is uniformly distributed among the windows. Window average data acquisition in this case would require (25 windows/blade) by (40 blades) by (5 data words/window), or 5000 words of storage. In contrast, data capture acquisition would require (25 windows) by (40 blades) by (100 meas./window) by (2 words/meas.), or 200 000 words of storage.

If DMA data transfer is used, sorting of velocity measurements into a data array which is addressed according to window number cannot be done in real time, but must be performed either after data acquisition is complete or in parallel with data acquisition. Implementation of real-time data display when using data capture methods therefore requires use of a multitasking computer operating system or an interruption of data acquisition for calculation of real-time displays. These issues are becoming less important as the cost of computer hardware and software capability continues to fall.

The ultimate acquisition approach would be to implement data acquisition algorithms which can automatically screen the probability density distribution acquired in each window during capture mode acquisition. If the distribution is well-behaved (i.e., nearly Gaussian), little information is lost by simply recording the distribution mean and standard deviation. The output of such an intelligent data capture method would therefore consist of probability density distributions for those measurement windows in which nonGaussian distributions were detected.

Total Number of Measurements Required

Two data acquisition issues which remain to be addressed are:

(1) how many measurement windows are required across a blade passage,

(2) how many measurements are needed to establish statistical confidence in the data.

The number of measurement windows required for accurate definition of the flowfield is dependent on the magnitude of the velocity gradients in the blade-to-blade direction. These gradients are averaged out across a measurement window during data acquisition since measurements which occur anywhere within a window are effectively assigned to the center of the window. Figure 20 shows a blade-to-blade Mach number distribution measured near the tip of a transonic fan blade in which a two-shock passage shock system is present. The measurements were acquired using 50 measurement windows across the passage. The Mach number distribution shown is the average of the distributions which exist in each of the 17 blade passages in which measurements were acquired. In Fig. 20 the second shock is clearly defined when $N_{window} = 50$. Also shown in Fig. 20 are the Mach number distributions which would result from using 25 and 12 windows across the blade pitch. Although the impact of reducing N_{window} to 25 is minimal, a value of N_{window} of 12 leads to an almost total smearing of the second shock and does not show the Mach number increase near the pressure surface. Note that method (4) discussed in the previous section concerning measurement of blade rotational position allows one to refine window resolution during post processing of the data. The other methods of measuring blade position require the user to fix the window resolution during the measurement process.

As discussed in the section on statistical measurement errors above, the number of measurements required to establish a given level of statistical confidence in the mean velocity, V, is related to the turbulence intensity. The number of measurements required as a function of turbulence intensity was summarized in Table I for various values of turbulence intensity at the 95 percent confidence level.

While a turbulence level of 5 percent is not uncommon in the core flow regions of turbomachinery blade flowfields, the turbulence intensity level within wakes can rise as high as 20 percent. If one desires to establish a 1 percent confidence interval in the mean velocity in a flow with a 5 percent turbulence level, then 100 measurements are required for each window. Acquisition of data across 1000 win-

dows would therefore require a total number of 100 000 measurements to achieve the desired accuracy in each window if the number of measurements were uniformly distributed across all of the measurement windows. In reality the measurements are not uniformly distributed, as shown in Fig. 21 which shows the distribution of the number of measurements which occurred during the measurement of the Mach number distribution previously shown in Fig. 20. One is therefore left with one of two choices:

(1) Collect data until the desired number of measurements are achieved in each window.

(2) Collect the desired total number of measurements and accept an increase in statistical error in those windows which have less than the desired number of measurements.

For typical applications, in which the time for data acquisition is of concern, the second choice is more practical than the first.

On-Line Data Monitoring

The use of on-line data reduction and display can greatly increase the effective use of an LA system in any application even if the data acquisition process is not totally automated. On-line feedback from the measurement process can indicate the presence of poor quality data and can also be used to ensure the capture of relevant flow features.

Figure 22, adapted from Ref. 22, shows one possible real-time display. This display is generated during a data acquisition process which uses 50 windows per blade passage across 20 blade passages. The display is updated every 10 to 15 sec during a run and is based on the data acquired up to that point in the run. The actual real-time display is shown in the center of Fig. 22 and is composed of the upper and lower plots shown in the figure. The upper plot is a plot of the velocity profile averaged across a blade pitch, i.e., it is calculated by averaging together measurements made in all of the individual blade passages. The blade suction surface is on the left side of the plot and the blade itself appears as the cross-hatched region on the right side of the plot. The lower plot in Fig. 22 is a bar graph which shows the number of measurements acquired in each of the 1000 measurement windows. The 20 gaps in the plot are caused by the 20 blades since no measurements are acquired as the blade passes through the incident laser beams. The accumulation of dirt and fluorescent seed material on the surface of the ninth blade passage is causing a large number of measurements due to light scattering from the blade surface.

While a real-time data display can be used to assess the quality of the data at individual survey locations, a rapid analysis of survey results is needed to ensure the capture of relevant global flow features. Use of on-line data analysis can reveal important data points which may have been missed during a survey. These data points can then be acquired while the research rig is still operating under the same conditions during which the survey was performed. An example of a case in which such a procedure would be useful is shown in Fig. 23 for a test run in which the objective is to map out the shock location in a transonic compressor rotor. The plot shown in the figure is a streamwise plot of relative Mach number created by plotting data acquired from several axial locations along line S-S during a flowfield survey. Results from the initial survey, shown on the left, indicate that the front passage shock lies somewhere between 10 and 20 percent chord and that the rear passage shock lies somewhere between 30 and 40 percent chord. If such a plot is available during the research run, the LA operator can make additional surveys in these regions in order to more accurately determine the shock location. The results of such additional surveys, shown on the right in Fig. 23, indicate that the actual front passage shock location is at 15 percent chord.

Sophisticated data acquisition methods which feature automated data acquisition and on-line data analysis require relatively sophisticated minicomputers for successful implementation. Use of 32-bit minicomputers with multitasking operating systems enables large data preparation, data acquisition, and data reduction programs to be core-resident at the same time, enables sharing of data between such programs, and enables concurrent execution of such programs. Large minicomputers also provide the speed required to implement on-line analysis of data acquired in a "data capture" mode. This analysis can provide on-line indication of flow features such as shock unsteadiness and wake vortex streets. Use of 16-bit minicomputers requires that large data acquisition programs be subdivided and "overlayed" in memory due to core storage addressing limitations. The slower execution speed of these smaller computers also limits the researcher to the use of the more efficient averaging methods of data acquisition discussed above which are not capable of resolving certain flow features. Successful LA measurements can also be acquired in turbomachines using 8-bit microcomputers. The type of hardware and software required between these two extremes depends on the level of information and the amount of information which one wishes to extract from the LA measurements.

ANALYSIS OF TURBOMACHINERY FLOWFIELDS USING LASER ANEMOMETER MEASUREMENTS

A number of different data acquisition methods of varying levels of complexity were discussed above. It was shown that data acquisition schemes can be simplified by employing some level of data averaging during the measurement process. However, such averaging prevents the extraction of certain levels of information from the flowfield. In this section an analogous situation will be shown to exist for both data analysis and graphical data display methods. A variety of methods will be presented and illustrated using examples from published results on laser anemometer applications to turbomachinery experiments.

The Hierarchy of Information Obtainable from LA Data

The process of analyzing LA data can be schematically represented by the informational pyramid shown in Fig. 24. The greatest amount of information is at the base of the pyramid. Successive application of averaging operators leads one to the peak of the pyramid. However, detailed information on flow features is lost as one moves to higher levels of the pyramid.

When performing an analysis of the variance in LA measurements acquired from flowfields generated within rotating turbomachinery one must be mindful of the periodicity present in the flowfield. In sta-

tionary, ergodic flows, one usually equates the level of measurement variance with the level of random flow fluctuations due to turbulence. As will be shown below, there is at least one contribution to the measurement variance which is not related to turbulence at each level of the pyramid.

The principles discussed above will be illustrated by analyzing an actual LA data set. This data set was acquired one-half chord downstream of an axial flow fan with a one-component LA system using 50 measurement windows between each blade. Measurements were recorded in 17 of the 22 fan blade passages. The total number of measurements recorded was 30 000, which yielded an average of about 40 measurements in each window. The velocity component measured is that which is in the streamwise direction outside of the blade wakes.

Analysis of Measurement Mean and Variance

The base of the informational pyramid contains the individual velocity measurements acquired in a capture mode of data acquisition. This data can be visualized as a two dimensional array V(i,j). The measurement window number, i, ranges between 1 and NW = NWP*NB, where NW is the total number of measurement windows, NWP is the number of windows per blade passage, and NB is the number of blade passages surveyed. In the example data set being used here, NW = 50, NB = 17 and NWP = 850. The index j ranges between 1 and N(i), the total number of measurements in window number i. As shown in Fig. 25, this data can be presented in the form of a velocity probability density distribution (p.d.d.) for each measurement window by classifying the N(i) velocity measurements into velocity bins of fixed width. Although p.d.d.'s can be generated for each measurement window, there are not enough measurements in an individual window in this data set to given an accurate description of the bimodal character of the p.d.d.'s which lie in the blade wake (point A). The p.d.d.'s shown in Fig. 25 therefore contain measurements acquired within the measurement windows located at points A and B in all 17 measured blade passages, and are therefore "blade average" p.d.d.'s. As shown in Ref. 27, the bimodal character of the p.d.d. at point A indicates that a vortex street is present in the blade wake.

Time averaging of the data acquired in each window leads to the second level of the informational pyramid, which contains the time-average circumferential velocity distribution between individual rotor blades, $\bar{V}(i)$. This velocity distribution can be directly acquired using a "window average" data acquisition technique or can be calculated from capture mode data using the averaging operation

$$\bar{V}(i) = \frac{1}{N(i)} \sum_{j=1}^{N(i)} V(i,j) \qquad i = 1,\ldots, NW \tag{1}$$

Note that $\bar{V}(i)$ is the statistical mean of the probability density distribution of the measurements from window number i.

The time-averaging operation also allows one to calculate the standard deviation, $\sigma_r(i)$, of the probability density distribution in window number i. This standard deviation is the lowest level of rms velocity information available (see Fig. 24) and can be calculated using the formula

$$\sigma_r^2(i) = \frac{1}{N(i) - 1} \sum_{j=1}^{N(i)} \left[\bar{V}(i) - V(i,j)\right]^2 \qquad i=1,\ldots,NW \tag{2}$$

Once the data is time-averaged, detailed information concerning the p.d.d. of the individual measurements which occurred in the measurement window is lost. However, the general level of broadening in the p.d.d. is indicated by the magnitude of $\sigma_r(i)$. In addition, information on passage-to-passage variation in the flowfield is still present in the data. Examples of the circumferential velocity distribution given by Equation (1) are shown in Fig. 26 across 2 of the 17 measured passages. The flags at selected points indicate the magnitude of the standard deviation σ_r. Note that the standard deviation rises in the wake as one would expect due to viscous mixing. However, the standard deviation alone does not indicate the vortical nature of the wake flow as inferred by the p.d.d. shown in Fig. 25. This information, which was contained in the p.d.d.'s has been lost due to averaging.

Now let us consider the factors which contribute to the variance σ_r. In a steady, laminar flow, all measurements in a probability density distribution would fall into the same velocity bin. In reality, the p.d.d. is broadened by the following mechanisms:

(1) Random turbulent fluctuations in the flow,

(2) Flow unsteadiness which occurs at frequencies which are not integral multiples of the rotor rotational frequency (such as rotor shock oscillations and trailing edge vortex shedding),

(3) Averaging of velocity gradients across the width of the measurement window,

(4) Flow variations caused by rotor speed drift during data acquisition,

(5) Individual LA measurement errors.

The contributions of items (2) to (5) must be subtracted from the standard deviation $\sigma_r(i)$ calculated from the p.d.d. in order to obtain the level of turbulent flow fluctuations. The LA user can control or can estimate the magnitude of some of the elements in items (2) to (5) above.

The contribution of item (3) can be minimized by reducing the physical size of the measurement window. The contribution of item (5) can be controlled by selecting the fringe orientation angles and the number of measurements so as to minimize the statistical measurement error. Individual LA measurement

errors arising from particle tracking errors can be minimized by generating uniformly small seed particles. As discussed in Ref. 9, the combined contributions of items (3) and (4) are on the order of 1 to 2 percent for a practical application.

Application of a spatial ensemble averaging process to the circumferential velocity distribution $\bar{V}(i)$ leads to the third level of the informational pyramid, which contains the ensemble-averaged velocity distribution $\tilde{V}(k)$. The ensemble averaging operation is given by

$$\tilde{V}(k) = \frac{1}{NB} \sum_{m=0}^{NB-1} \bar{V}(k + m.NWP) \quad k=1,\ldots,NWP \tag{3}$$

This ensemble averaged velocity distribution can be directly acquired using a "blade average" data acquisition technique in which NWP windows are generated between successive blade passing signals. The $\tilde{V}(k)$ velocity distribution contains information on the circumferential variation in the flowfield across an "average" blade passage. Detailed information on the variation of the flowfield between individual blade passages is lost. This information is lumped into the standard deviation $\sigma_g(k)$ at each point in the ensemble-averaged velocity distribution, given by

$$\sigma_g^2(k) = \frac{1}{NB - 1} \sum_{m=0}^{NB-1} [\tilde{V}(k) - \bar{V}(k + m.NWP)]^2 \quad k=1,\ldots,NWP \tag{4}$$

Fig. 27 is an illustration of the ensemble-averaged velocity distribution calculated from the example data set by averaging across the 17 measured blade passages. The flags shown on selected points indicate the magnitude of the rms velocity σ_g.

This rms velocity arises from passage-to-passage flow variations. This geometric contribution to rms velocity fluctuations can be seen in Fig. 28, where the individual velocity distributions across the 17 measured blade passages are plotted to the same scale.

The fourth level of the informational pyramid contains the pitchwise-averaged velocity $\bar{\bar{V}}$. This velocity can be obtained from the spatially ensemble-averaged velocity using the averaging operation

$$\bar{\bar{V}} = \frac{1}{NWP} \sum_{k=1}^{NWP} \tilde{V}(k) \tag{5}$$

The standard deviation of $\bar{\bar{V}}$ is calculated using

$$\sigma_p^2 = \frac{1}{NWP - 1} \sum_{k=1}^{NWP} [\bar{\bar{V}} - \tilde{V}(k)]^2 \tag{6}$$

The values of $\bar{\bar{V}}$ and σ_p calculated from the ensemble-averaged velocity distribution are included in Fig. 27. This information can be directly acquired by a simple LA system which contains no capability for measuring rotational position of moving blade rows. All details concerning the blade-to-blade flowfield are lost at this level of averaging. Data of this type is of interest when comparing LA measurements to those obtained with aerodynamic instrumentation such as total and static pressure probes and thermocouples whose frequency response is well below the blade passing frequency. The time-average velocity at the measurement point is also used when measuring the steady state flowfield in stationary blade rows.

At the top of the informational pyramid, the variance in the pitchwise-average velocity, σ_t, contains contributions from all lower levels of the pyramid. Several authors (Refs. 28 to 30) have addressed this issue in the past using a model similar to that shown in Fig. 29. These investigators have shown that the total rms velocity at the measurement point, σ_t, is related to the random fluctuation level and the periodic fluctuation level σ_p by the relation

$$\sigma_t^2 = \sigma_r^\sigma + \sigma_p^2$$

These investigators have assumed that the flowfield is the same in each blade passage. If however, there are flowfield variations from passage-to-passage, such that the velocity distribution $\bar{V}(i)$ in each passage is not identical to the ensemble-averaged distribution $\tilde{V}(k)$, an additional contribution σ_g must be included:

$$\sigma_t^2 = \sigma_r^2 + \sigma_p^2 + \sigma_g^2$$

It should be noted that calculation of the ensemble-averaged profile, $\tilde{V}(k)$, can be performed directly from the individual velocity measurement array $V(i,j)$. It should also be noted that the pitchwise-averaged velocity, $\bar{\bar{V}}$, is identical to the arithmetic average of all measurements in the $V(i,j)$ array. The calculation of $\tilde{V}(k)$ in terms of $\bar{V}(i)$ shown in equation (3) and the calculation of $\bar{\bar{V}}$ in terms of $\tilde{V}(k)$ shown in equation (5) was done in order to more clearly show how information is lost during each averaging operation. The following formulas can be used for direct calculation of $\tilde{V}(k)$ and $\bar{\bar{V}}$:

$$\tilde{V}(k) = \frac{\left[\sum_{m=0}^{NB-1} \sum_{j=1}^{N(k+m\cdot NWP)} V(k + m\cdot NWP, j)\right]}{\left[\sum_{m=0}^{NB-1} N(k + m\cdot NWP)\right]} \quad k=1,\ldots,NWP$$

$$\bar{V} = \frac{\left[\sum_{I=1}^{NW}\sum_{J=1}^{N(I)} V(I,J)\right]}{\left[\sum_{I=1}^{NW} N(I)\right]} \qquad NW = NWP.NB$$

Care must be taken when computing all of the averages discussed above, since the velocity is a vector which has both magnitude and direction. This point can be seen more clearly by considering the averaging of the two vectors shown in the diagram below:

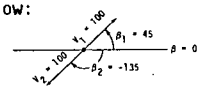

The actual average velocity obtained by vector addition is of course zero. However, if one averages the velocity magnitude and angle separately one gets

$$V_{av} = \frac{(V_1 + V_2)}{2} = 100$$

$$\beta_{av} = \frac{(\beta_1 + \beta_2)}{2} = \frac{(45 - 135)}{2} = -45$$

which is incorrect.

The proper method of calculating average values of any velocity triangle parameter is to average the primary velocity components V_x and V_y first, and then calculate the desired quantity. In the above illustration this would lead to

$$(V_x)_{av} = \frac{(V_{x1} + V_{x2})}{2} = \frac{(71.7 - 71.7)}{2} = 0$$

$$(V_y)_{av} = \frac{(V_{y1} + V_{y2})}{2} = \frac{(71.7 - 71.7)}{2} = 0$$

The proper method of calculating the ensemble-averaged flow angle, $\beta(k)$, for example is therefore:

$$\tilde{V}_z(k) = \sum_{m=0}^{NB-1} \bar{V}_z(k+m.NWP) \qquad \tilde{V}_\theta(k) = \frac{1}{NB}\sum_{m=0}^{NB-1} \tilde{V}_\theta(k+m.NWP) \qquad k=1,\ldots,NWP$$

$$\tilde{\beta}(k) = \text{ARCTAN}\left[\frac{\tilde{V}_\theta(k)}{\tilde{V}_z(k)}\right] \qquad k=1,\ldots,NWP$$

This same procedure applies to other velocity triangle parameters such as relative and absolute velocity magnitude and relative flow angle.

The preceding discussion indicates that the level of information which one wishes to extract from the flowfield can be used to determine both the type of data acquisition method used and the level of averaging employed during data post-processing. Although information is lost through averaging as one proceeds up the pyramid shown in Fig. 24, substantial savings in data acquisition time, data processing time, and data storage space can be realized at the upper pyramid levels. For example, let NR be the number of measurements required to describe the velocity to a certain level of confidence at each point in the circumferential velocity distribution $\bar{V}(I)$. In keeping with the example used above, let the total number of windows be NW=850, corresponding to 50 windows per blade across 17 blades. The total number of measurements required is therefore NT=NR*NW = 850*NR. If, however, one is only interested in the ensemble averaged velocity $\tilde{V}$ or the time average velocity $\bar{V}$, then the same level of confidence requires only 50*NR and NR measurements respectively.

Continuing with the above example, one cannot hope to assimilate all of the information contained in the p.d.d.'s for each of the 850 measurement windows. Consideration of the circumferential velocity distribution, $\bar{V}(I)$ across 17 blade passages at each axial, radial survey location within the blade row can also be quite tedious. Therefore, in practice one usually resorts to detailed consideration of one of the following:

(1) The distribution of $\bar{V}(I)$ across a few individual blade passages if passage-to-passage flow variations are large.

(2) The distribution of $\tilde{V}(k)$ across the ensemble-averaged blade passage if passage-to-passage flow variations are small.

Graphical Methods of Data Presentation

Several different methods of presenting the data accumulated along the circumferential measurement line swept through a rotating blade row at one axial, radial survey location have been presented in the preceding sections. Additional graphical methods are required when attempting to visualize global flow features.

Shock wave locations in transonic blade rows can be determined from a series of blade-to-blade plots of data acquired at different streamwise locations. An independent determination of shock location can also be achieved by streamwise cross-plotting of data obtained at a constant pitchwise distance. These combined procedures are illustrated in Fig. 30. Although the seed particle velocity may lag the gas velocity for a short distance downstream of the shock, the point at which the measured velocity first begins to decrease provides a consistent measure of the shock front location.

In contrast to the one-dimensional slices through the flowfield offered by blade-to-blade and streamwise plots, contour plots offer the user a two-dimensional view of the flowfield. An example of a contour plot of the Mach number distribution in a transonic axial-flow fan is shown in Fig. 31. Contour plots are often used when comparing LA measurements to results generated by numerical flow analysis codes.

Changes in the magnitude of a flow parameter are more easily discerned from one-dimensional plots such as those in Fig. 30 than from contour plots. This is due to the fact that one must visually integrate across contour lines to determine magnitude changes when viewing contour plots. As a result, contour plots tend to be more qualitative than quantitative. This situation can be improved by three-dimensional plotting which adds parameter magnitude to contour plots as a third dimension. The use of varying viewing angles, perspective, and hidden line techniques can greatly enhance the information obtainable from three-dimensional plots, as shown by the examples in Fig. 32. The valley-like features ahead of the blade row represent the Mach number variation caused by bow waves from adjacent blades. The passage shock location is clearly shown in the lower part of Fig. 32.

Example Results from LA Applications in Turbomachinery

Published results from LA investigations will be briefly reviewed below in order to demonstrate the capabilities of the LA technique. The examples will be limited to axial-type turbomachines. A more complete list of examples from axial-flow turbomachinery experiments is given in Ref. 31. An excellent summary of LA applications in radial-type machines has recently been given by Krain (Ref. 2). In addition, results obtained in radial-flow turbomachinery will be discussed in this symposium by Schodl and Elder (Refs. 3 and 4).

Passage-To-Passage Flow Variations

An ideal turbomachine would produce an identical flowfield in each blade passage in the blade row. However, manufacturing tolerances limit the degree to which real machines approach this ideal goal. Passage-to-passage flow variations measured in two transonic fan rotors are shown in Fig. 33 in the form of blade-to-blade distributions of relative Mach number in individual blade passages. The blade suction and pressure surfaces are denoted by SS and PS, respectively. The results shown in Fig. 33(a) were obtained in a 550 m/sec tip speed fan with an aspect ratio of 2.87 which had a part-span damper. The results shown in Fig. 33(b) were obtained in an undampered 1.56 aspect ratio fan with a tip speed of 429 m/sec. The Mach number distributions shown in Fig. 33(a) for blade passages 1 and 15 encompass the range of those measured in each of the 38 individual blade passages. Note that the flowfield in passage 15 is representative of an oblique shock while the flowfield in passage 1 indicates the presence of a normal shock. Analysis of data from additional fans has led to the conclusion that the large variations shown in the dampered fan flowfields arise due to variations in blade geometry caused by manufacturing variations in the dampers. Another feature which appears in Fig. 33 is the improved flowfield uniformity at the near stall operating condition shown in Fig. 33(b). This phenomena has also been observed in data from other LA experiments and appears to be a general behavior of transonic fans. Large passage-to-passage flowfield variations have two important impacts:

(1) They generate an increased level of apparent turbulence to downstream blade rows as represented by the rms velocity σ_g discussed in the previous section.

(2) They make numerical flowfield analysis difficult because there is no single blade passage in which the flow can be considered to be representative of the flow throughout the blade row.

Unsteady Flow Features in Isolated Rotors

The capture mode of data acquisition allows detection of flow fluctuations with frequencies which are not integral orders of the once-per-rev frequency. One example of this capability is the detection of vortices in the blade wake as inferred from the double-peaked probability density distribution shown in Fig. 25. Another example of this capability is shown in Fig. 34. which is taken from Ref. 19. The bimodal nature of the probability density functions shown in Fig. 34 indicates an oscillation of the rotor passage shock about the mean location shown in the upper part of the figure. The bimodal p.d.d.'s obtained in windows C and D are due to the fact that these windows lie upstream of the shock part of the time and downstream of the shock part of the time.

Blade Row Interactions

The unsteady flow features just discussed occurred in isolated rotors where the flowfield should nominally be axisymmetric and steady in the rotor relative frame of reference. When a rotor is followed by a stator, the flowfield is unsteady and nonaxisymmetric in both the relative and absolute frames of reference. An investigation of the periodically unsteady flow through a stationary blade row therefore requires a circumferential survey across one blade pitch in the stationary blade row. The array of survey locations used during the experiment reported in Ref. 32 to investigate the flow through a stator located downstream of a compressor rotor is shown in Fig. 35. Note that a total of 128 survey points were used in order to survey the flow at 15 axial locations, which represents an eightfold increase in the number of survey locations which would have been required if the flow was axisymmetric. Data acquired at each pitchwise location must still be tagged with the rotor rotational position. By plotting the velocities measured at each axial and circumferential location for a given rotor rotational position one obtains a snapshot of the periodically unsteady flow through the stator. Figure 36 illustrates this procedure for three different pitchwise locations of the rotor relative to the stator. Turbulence intensity is chosen

as the plotted parameter in this case in order to clearly define the rotor wake location. The rotor wake is sheared as it convects through the stator passage due to the fact that the velocity is higher on the suction side of the passage than on the pressure side of the passage. A similar analysis of turbine vane wakes passing through a turbine rotor has been reported in Refs. 30 and 33.

The above investigations were performed in single stage machines. Measurements acquired within a multistage axial flow compressor using the laser transit technique have been reported in Ref. 34. The application of the LFA technique to a high speed multistage axial compressor will be discussed in this Symposium by Williams (Ref. 35).

CONCLUDING REMARKS

During the last 14 years laser anemometry has been shown to be a viable technique for obtaining detailed internal flow measurements from within the hostile turbomachinery environment. Advances in optics, electronics, and computer technology during this time have led to the availability of commercial, off-the-shelf laser fringe and laser-transit anemometer systems for use in turbomachinery investigations. Future advancements in LA applications will therefore depend on improvements in the following areas:

(1) The efficient acquisition, analysis, and display of the large amount of data which can be produced during LA applications,

(2) Measurement of the radial velocity component which usually lies in the line-of-sight direction of the LA system,

(3) Acquisition and analysis of data from within multistage turbomachines,

(4) Use of flow visualization techniques such as holography and trace gas injection to scope global flow features in order to reduce the number of physical locations at which LA measurements must be acquired,

(5) Accurate measurement of turbulent and periodically unsteady flow fluctuations in turbomachinery in order to accurately assess the relative importance of random and coherent fluctuations,

(6) development of optical techniques for measurement of thermodynamic properties which can be used in conjunction with the LA technique to yield simultaneous measurement of velocity and density, pressure, or temperature.

REFERENCES

1. Wisler, D.C., and Mossey, P.W., "Gas Velocity Measurements Within a Compressor Rotor Passage Using the Laser Doppler Velocimeter," ASME Paper No. 72-WA/GT-2, (1972).

2. Krain, H., "Experimental Observation of the Flow in Impellers and Diffusers," Von Karman Lecture Series No. 7, 1984.

3. Schodl, R., "Laser Two Focus Velocimetry," AGARD CP-399, Advanced Instrumentation for Aero Engine Components, 1986.

4. Elder, R.L., Forster, C.P., and Gill, M.E., "Application of Doppler and Transit Anemometry in Small Turbomachines," AGARD CP-399, Advanced Intrumentation for Aero Engine Components, 19-23, 1986.

5. Seasholtz, R.G., "Laser Doppler Velocimeter System for Turbine Stator Cascade Studies and Analysis of Statistical Biasing Errors," NASA TN D-8297, 1977.

6. Lading, L., "The Time of Flight vs the LDA," Proceedings of the Third International Workshop on Laser Velocimetry, Purdue University, 1978.

7. Boutier, A., D'Humieres, Ch., and Soulevant, D., "Three Dimensional Laser Velocimetry: A Review," Second International Symposium on Applications of Laser Anemometry to Fluid Mechanics, Lisbon, Portugal, July 1984.

8. Boutier, A., "How to Choose a Laser Velocimeter for a Given Application," AGARD CP-399, Advanced Instrumentation for Aero Engine Components, 1986.

9. Strazisar, A.J., and Powell, J.A., "Laser Anemometer Measurements in a Transonic Axial Flow Compressor Rotor," ASME Journal of Engineering for Power, Vol. 103, No. 2, April 1981, pp. 430-437.

10. Larguier, R., "Experimental Analysis Methods for Unsteady FLows in Turbomachines," ASME Journal of Engineering for Power, Vol. 103, April 1981, pp. 415-421.

11. Reinath, M.S., Orloff, K.L., and Snyder, P.S., "A Laser velocimeter System for Large-Scale Aerodynamic Testing," NASA TM-84393, January, 1984.

12. Orloff, K.L., and Snyder, P.K., "Laser Doppler Anemometer Measurements Using Nonorthogonal Velocity Components: Error Estimates," Applied Optics, Vol. 21, January 1982, pp. 339-344.

13. Melling, A., "Seeding Gas Flows for Laser Anemometry," AGARD CP-399, Advanced Instrumentation for Aero Engine Components, 1986.

14. Stevenson, W.H., dos Santos, R., and Mettler, S.C., "Fringe Mode Fluorescence Velocimetry," AGARD CP-193, May 1976, pp. 21.1-21.9.

15. Seasholtz, R.G., and Goldman, L.J., "Three Component Velocity Measurements Using Fabry-Perot Interferometer," Second International Symposium on Applications of Laser Anemometry to Fluid Mechanics, Lisbon, Portugal, July 1984, (NASA TM-83692).

16. Seasholtz, R.G., and Goldman, L.J., "Laser Anemometer Using a Fabry-Perot Interferometer for Measuring Mean Velocity and Turbulence Intensity Along the Optical Axis in Turbomachinery," Engineering Applications of Laser Velocimetry, ASME Book No. H00230.

17. Seasholtz, R.G., and Goldman, L.J., "Combined Fringe and Fabry-Perot Laser Anemometer for Three Component Velocity Measurements in a Turbine Stator Cascade Facility," AGARD CP-399, Advanced Instrumen- tation for Aero Engine Components, 1986.

18. Wernet, M.P., and Edwards, R.V., "Implementation of a New Type of Time-of-Flight Laser Anemometer," Applied Optics, Vol. 25, No. 5, March 1986, pp. 644-648.

19. Strazisar, A.J., "Investigation of Flow Phenomena in a Transonic Fan Rotor Using Laser Anemometry," ASME Journal of Engineering for Power, Vol. 103, No. 2, April 1981, pp. 43-437.

20. Owen, A.K., "A Parametric Study of the Beam Refraction Problems Across Laser Anemometer Windows," Third International Symposium on the Application of Laser Anemometry to Fluid Mechanics, Lisbon, Portugal, July 7-9, 1986.

21. Schock, H.J., Case, S., and Konicek, L., "Window Aberration Correction in Laser Velocimetry Using Multifaceted Holographic Optical Elements," Applied Optics, Vol. 23, No. 5, march 1984, pp. 752-756.

22. Powell, J.A.,, Strazisar, A.J., and Seasholtz, R.G., "Efficient Laser Anemometer for Intra-Rotor Flow Mapping in Turbomachinery," ASME Journal of Engineering for Power, vol. 103, No. 2, April 1981, pp. 424-429.

23. Walker, D.A., Williams, M.C., and House, R.D., "Intrablade Velocity Measurements in a Transonic Fan Utilizing a Laser Doppler Velocimeter," Minnesota Symposium on Laser Anemometry, University of Minnesota, Minneapolis, October 22-24, 1975.

24. Schodl, R., "A Laser-Two-Focus (L2F) Velocimeter for Automatic Flow Vector Measurements in the Rotat- ing Components of Turbomachines," ASME Journal of Fluids Engineering, Vol. 102, December 1980, pp. 412-419.

25. Lepicovsky, J., and Bell, W.A., "Aerodynamic Measurements About a Rotating Propeller with a Laser Velocimeter," AIAA Journal of Aircraft, Vol. 24, No. 4, April 1984, pp. 264-271.

26. Fraser, S.M., and Carey, C., "Two-Dimensional Laser Doppler Anemometer Measurements in an Axial Flow Fan," presented at the International Symposium on Applications of Laser-Doppler Anemometry to Fluid Mechanics, Lisbon, Portugal, July 5-7, 1982.

27. Hathaway, M.D., Gertz, J., Strazisar, A.J., and Epstein, A.H., "Rotor Wake Characteristics of a Tran- sonic Axial Flow Fan," AIAA Paper 85-1133, 1985 (to be published in the AIAA Journal, 1986).

28. Evans, R.L., "Turbulence and Unsteadiness Measurements Downstream of a Moving Blade Row," ASME Paper No. 74-GT-73 (1975).

29. Joslyn, H.D., Dring, R.P., and Sharma, O.P., "Unsteady Three-Dimensional Turbine Aerodynamics," ASME Journal of Engineering for Power, Vol. 105, No. 2, April 1983, pp. 322-331.

30. Binder, A., Forster, W., Kruse, H., and Rogge, H., "An Experimental Investigation Into the Effect of Wakes on the Unsteady Turbine Rotor Flow," ASME Paper No. 84-GT-178 (1984).

31. Strazisar, A.J., "Application of Laser Anemometry to Turbomachinery Flowfield Measurements, Von Karman Lecture Series No. 3, 1985.

32. Dunker, R.J., "Flow Measurements in the Stator Row of a Single-State Transonic Axial-Flow Compressor with Controlled Diffusion Stator Blades," AGARD CP-351, Viscous Effects in Turbomachines, June 1983.

33. Binder, A., "Turbulence Production Due to Secondary Vortex Cutting in a Turbine Rotor," ASME Paper No. 85-GT-193.

34. Ding, K., "Flow Measurements Using a Laser-Two-Focus Anemometer in a High Speed Centrifugal and a Multistage Axial Compressor," Engineering Applications of Laser Velocimetry, ASME Book NO. H00230.

35. Williams, C., "Laser Velocimetry Study of a Stator-Rotor Interaction in a Multistage Gas Turbine Com- pressor," AGARD CP-399, Advanced Instrumentation for Aero Engine Components, 1986.

ACKNOWLEDGMENTS

The successful application of laser anemometry to turbomachinery research generally requires the efforts of many people. The author would therefore like to acknowledge the efforts of the following people at Lewis: Dick Seasholtz and Tony Powell for optical and electronic design, Karl Owen for the calculation of window refraction effects, Mike Pierzga, Michael Hathaway, Sue Simonyi, Ken Suder, and

Gary Skoch for acquiring and analyzing data. In addition, Carl Williams, Dick Schodl, Tony Smart, David Hobbs, and David C. Prince Jr. have provided many insights over the years into the acquisition and analysis of laser-transit and laser-fringe anemometer data in turbomachinery.

TABLE I. - NUMBER OF MEASUREMENTS REQUIRED FOR 95 PERCENT CONFIDENCE LEVEL IN MEASURED MEAN VELOCITY AND TURBULENCE INTENSITY

[N_V = number of measurements required for 95 percent confidence that the measured mean velocity is within C_V percent of the true mean velocity; $N_{V'}$ = number of of measurements required for 95 percent confidence that the measured turbulence intensity is within $C_{V'}$ percent of the turbulence intensity; V'/V = turbulence intensity.]

Mean Velocity Estimate				
Desired accuracy, $C_{V'}$, percent	Turbulence level, V'/V, percent			
	1	5	10	20
0.5	16	400	1600	6400
1.0	4	100	400	1600
2.0	1	25	100	400
5.0	--	4	16	64
10.0	--	1	4	16

Turbulence Intensity Estimate	
Desired accuracy, $C_{V'}$, percent	Number of measurements, $N_{V'}$
0.5	80 000
1.0	20 000
2.0	5 000
5.0	800
10.0	200

TABLE II. - LASER FRINGE ANEMOMETER BEAM REFRACTION EFFECTS ACROSS A CYLINDRICAL WINDOW

Window thickness, in.	Beam orientation angle, δ degrees	Beam crossing angle at the probe volume, degrees	Radial shift in p.v. location, ΔR in.	Beam uncrossing distance		
				Microns	No. of fringes	Percent of probe volume diameter
probe volume radius = 9.5 in.						
0.125	0	1.400	0.043	0	0	0
	45	1.403	.040	2.94	.28	2.4
.250	0	1.400	.086	0	0	0
	45	1.405	.080	6.63	.63	5.3
probe volume radius = 5.0 in.						
0.125	0	1.4000	0.043	0	0	0
	45	1.4015	.027	19.7	1.87	15.8
.250	0	1.4000	.086	0	0	0
	45	1.4025	.053	39.6	3.76	31.7

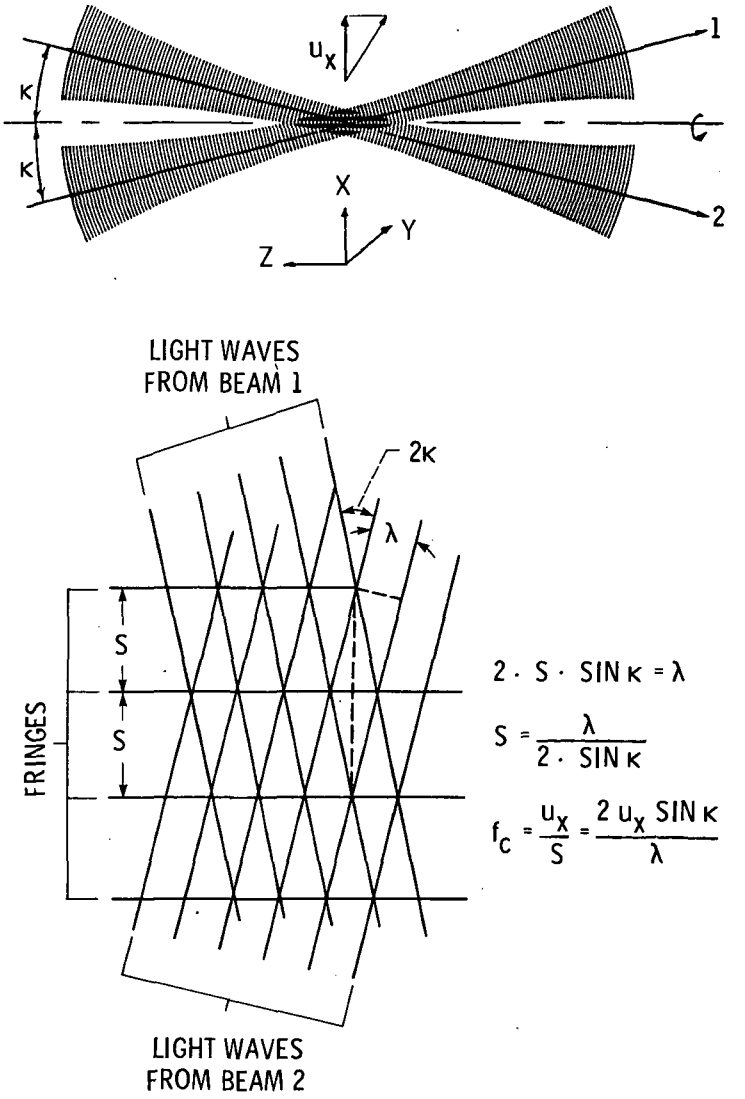

Figure 1. - Fringe model of a laser anemometer.

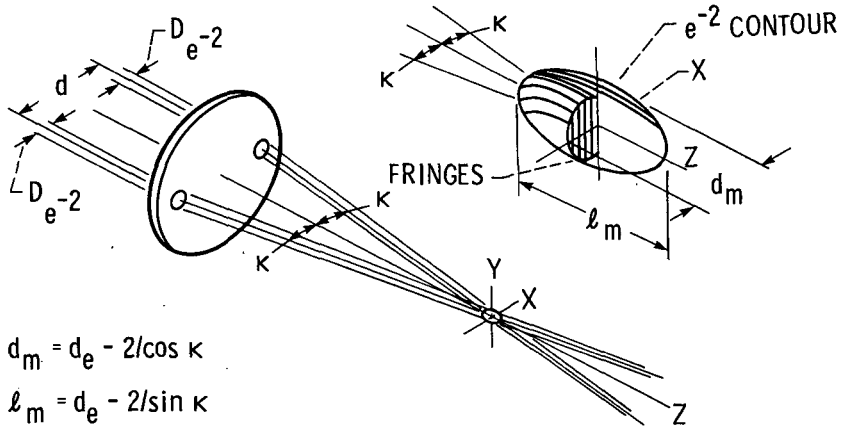

$$d_m = d_e - 2/\cos \kappa$$

$$\ell_m = d_e - 2/\sin \kappa$$

$$V = \pi d_e^3 - 2/(6 \cos \kappa \sin \kappa)$$

$$N_{FR} = \frac{d_m}{d_f} = \frac{1.27\, d}{D_{e^{-2}}}$$

Figure 2. - Geometry of a laser fringe anemometer.

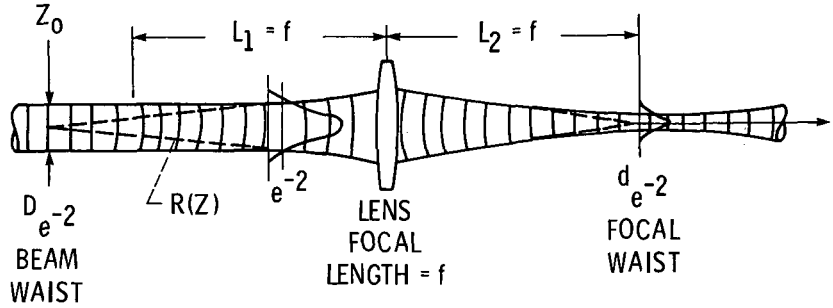

$$d_{e^{-2}} = 4\lambda f/\pi D_{e^{-2}}$$

Figure 3. - Properties of a Gaussian beam.

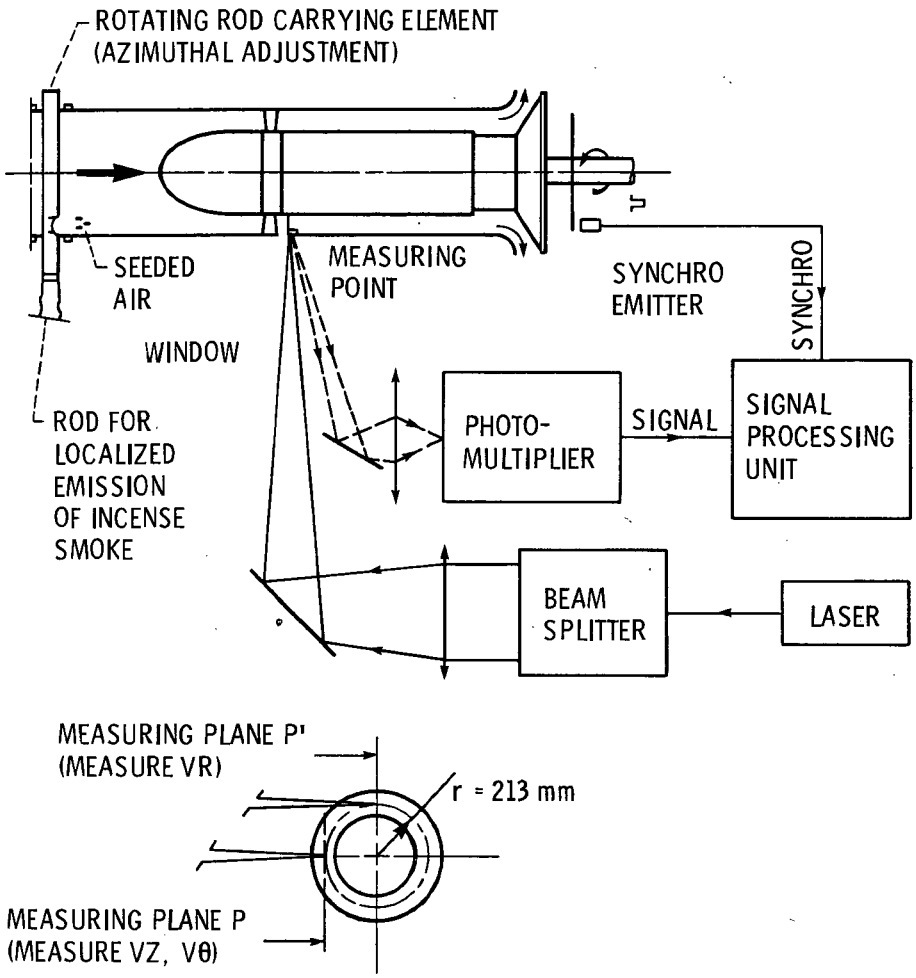

Figure 4. - Measurement of radial velocity components downstream of a compressor blade row. VZ, Vθ measured using window P. VR measured using window P'.

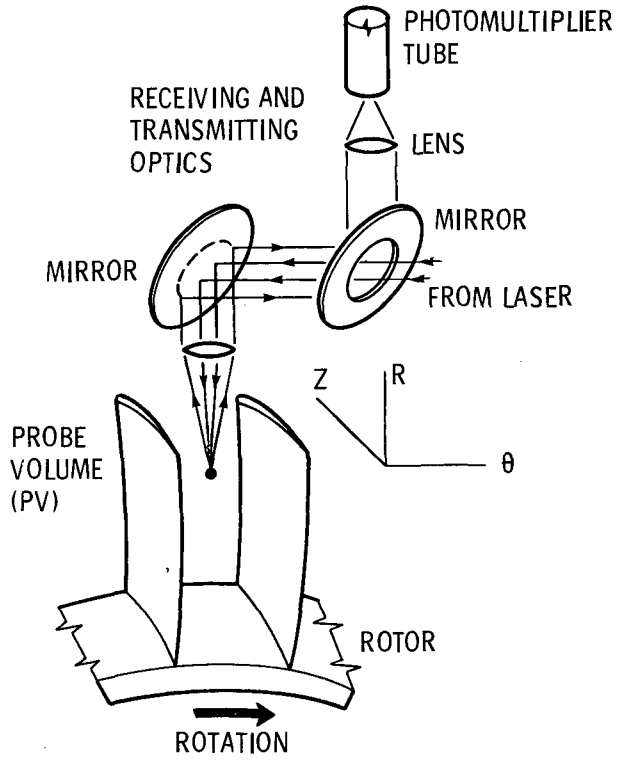

(a) Conventional system.

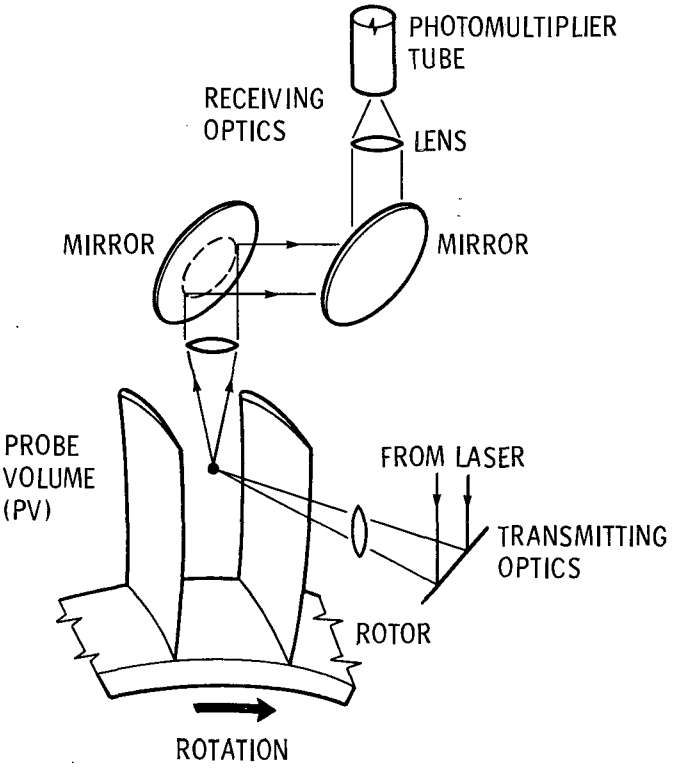

(b) Radial flow system.

Figure 5. - Measurement of radial velocity components within a blade row using off-axis light collection.

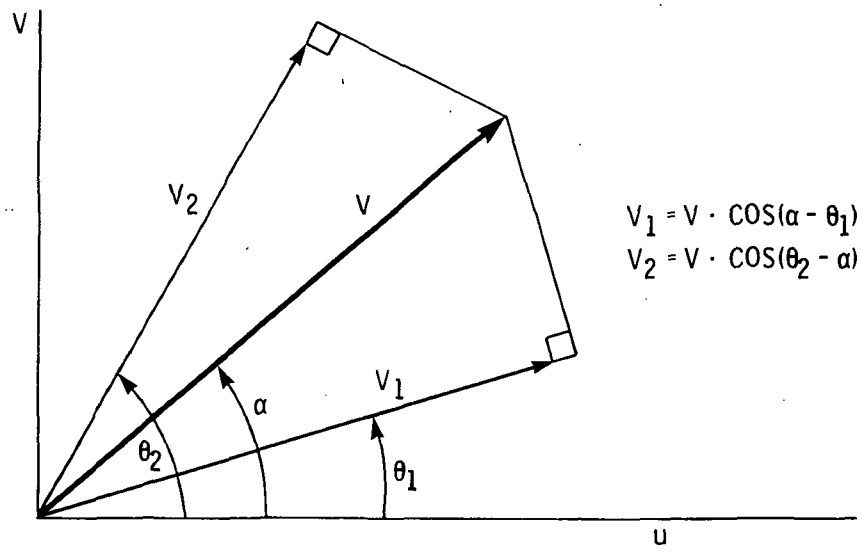

Figure 6. - Determination of unknowns V and α using velocities V_1 and V_2 measured at fringe orientations θ_1 and θ_2.

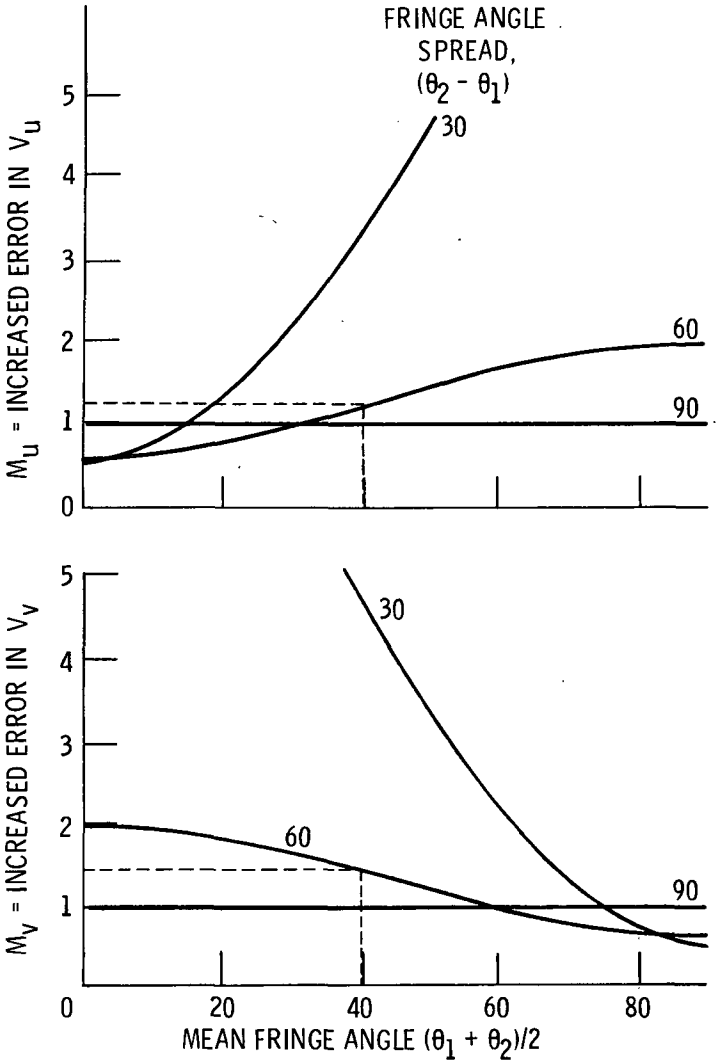

Figure 7. - Increase in statistical error due to use of uncorrelated measurements in calculating velocity components.

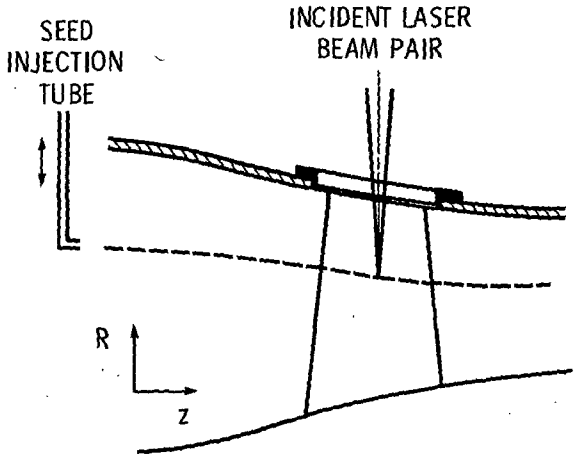

Figure 8. - Point injection of seed into streamtube passing through the measurement point.

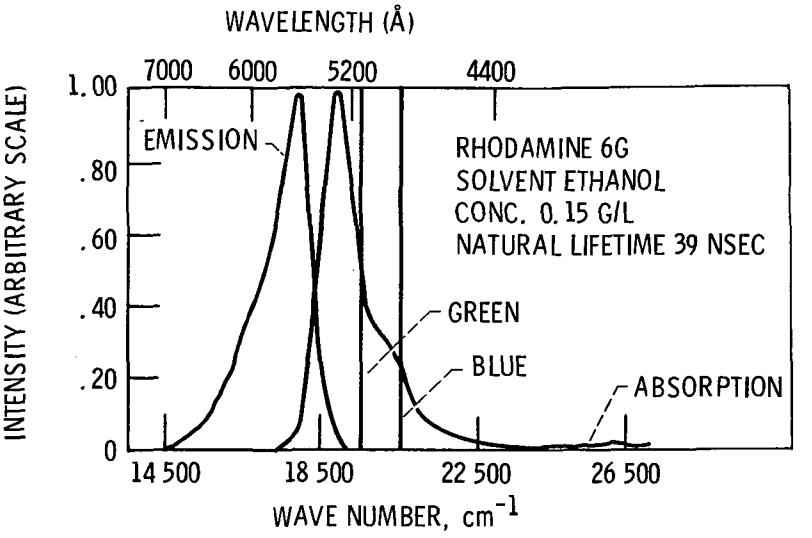

(a) Emission and absorption spectra.

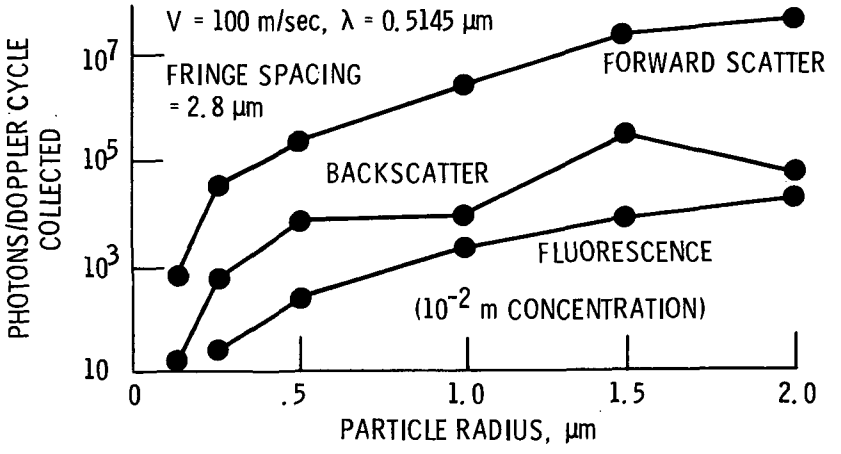

(b) Comparison between fluorescence emission and light scattering versus particle size.

Figure 9. - Characteristics of rhodamine 6G fluorescing dye.

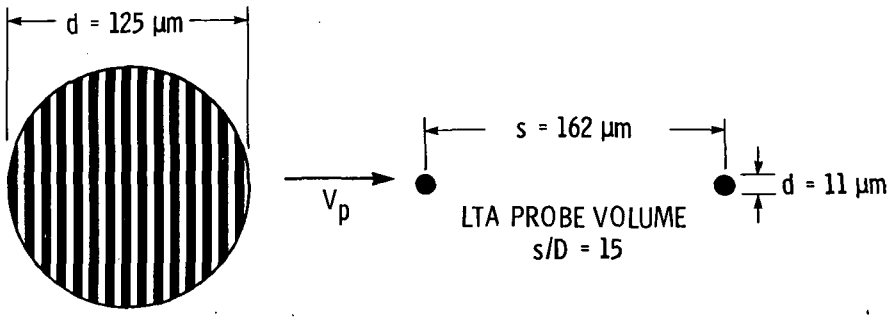

Figure 10. - Comparison of typical laser-fringe and laser-transit anemometer probe volumes.

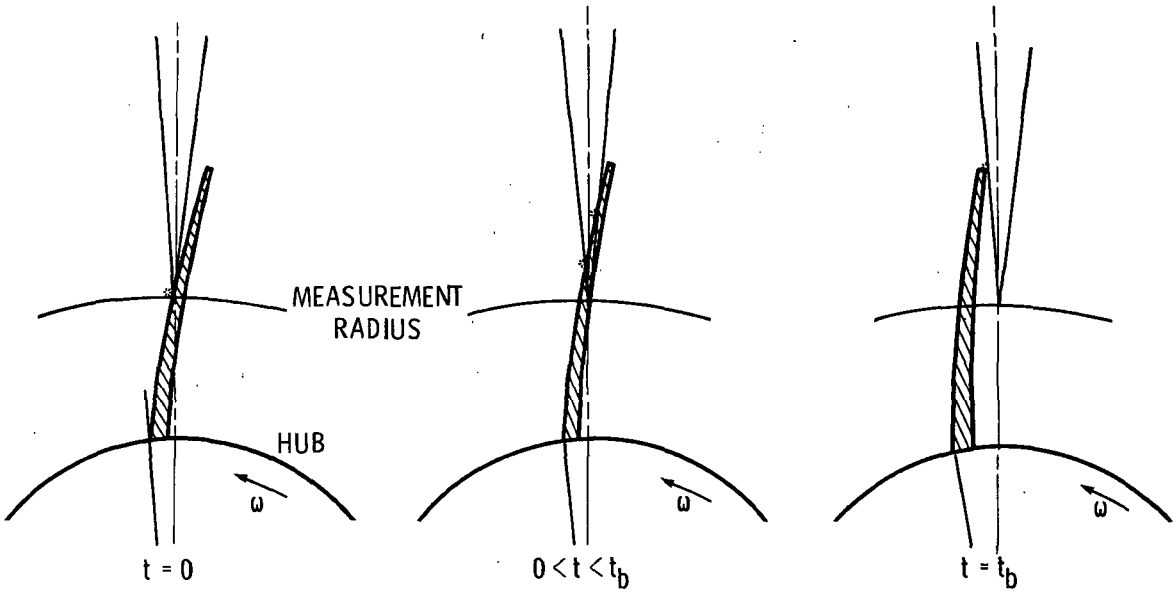

Figure 11. - Incident light reflection from blade surfaces.

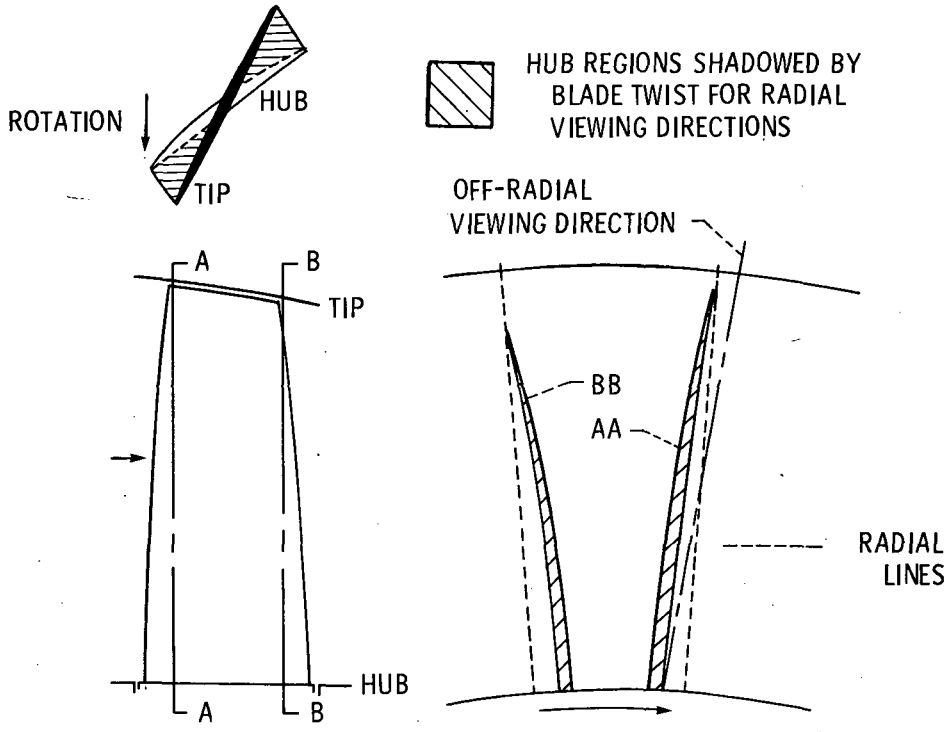

(a) Axial view. (b) View looking downstream.

Figure 12. - Existence of shadowed regions caused by blade twist.

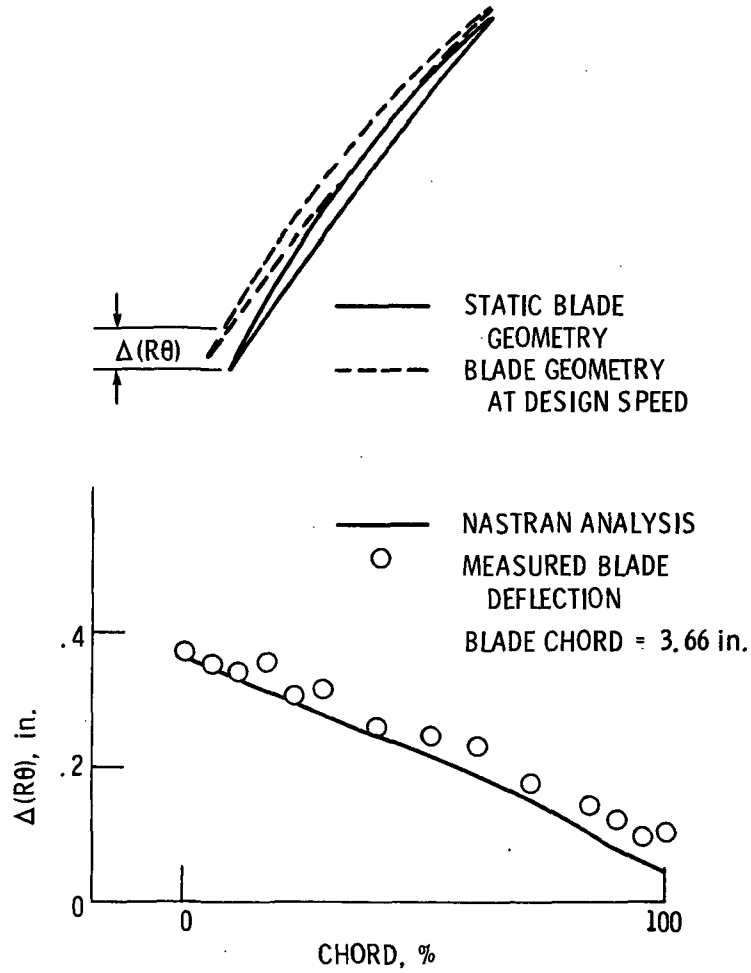

Figure 13. - Comparison of measured and predicted untwist at the tip of an axial flow fan at a tip speed of 429 m/sec.

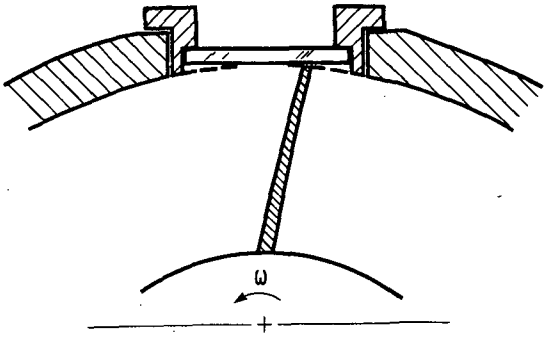

(a) Tip clearance distortion due to casing curvature.

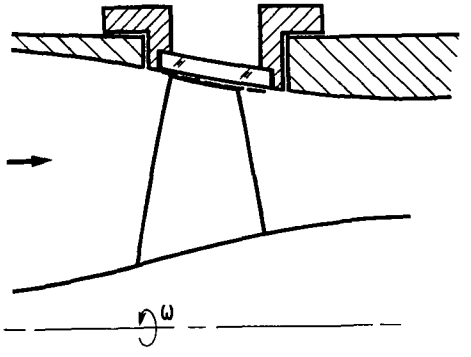

(b) Tip clearance distortion due to flow-path convergence.

Figure 14. - Flowpath distortions caused by flat windows.

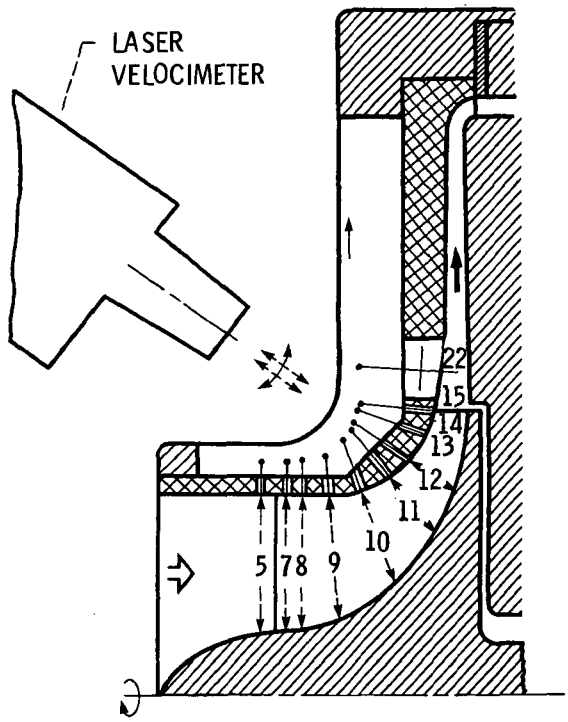

Figure 15. - Use of small flat windows in radial turbomachines to minimize flowpath distortions.

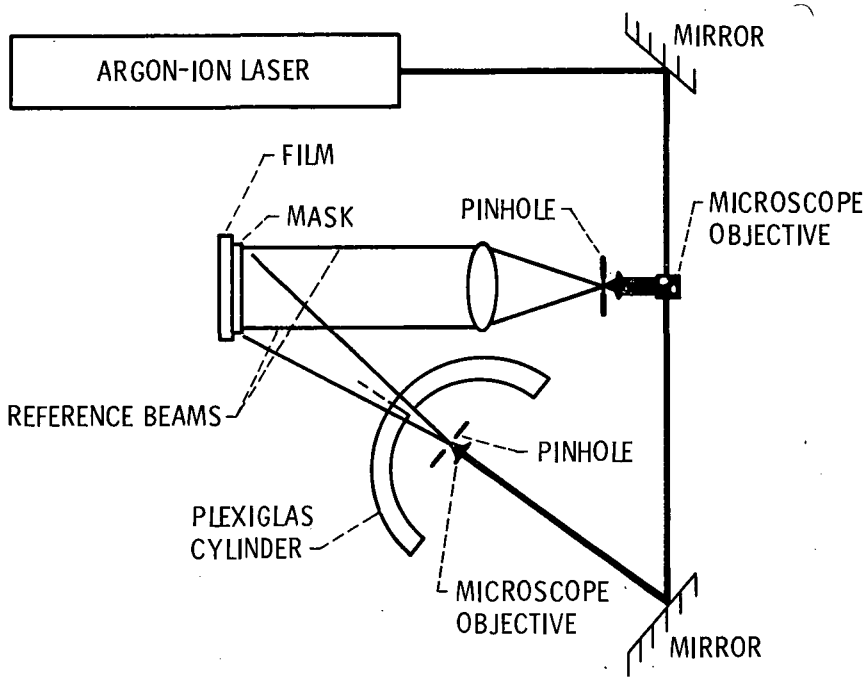

(a) Hologram construction. Pinhole is at the desired probe volume location.

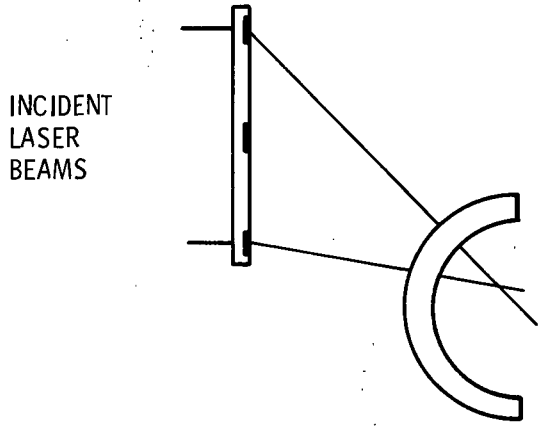

(b) Holographic refraction correction. Incident laser beams propagate through the hologram in the direction taken by the reference beam during hologram construction and cross at the desired probe volume location.

Figure 16. - Holographic correction of window refraction effects.

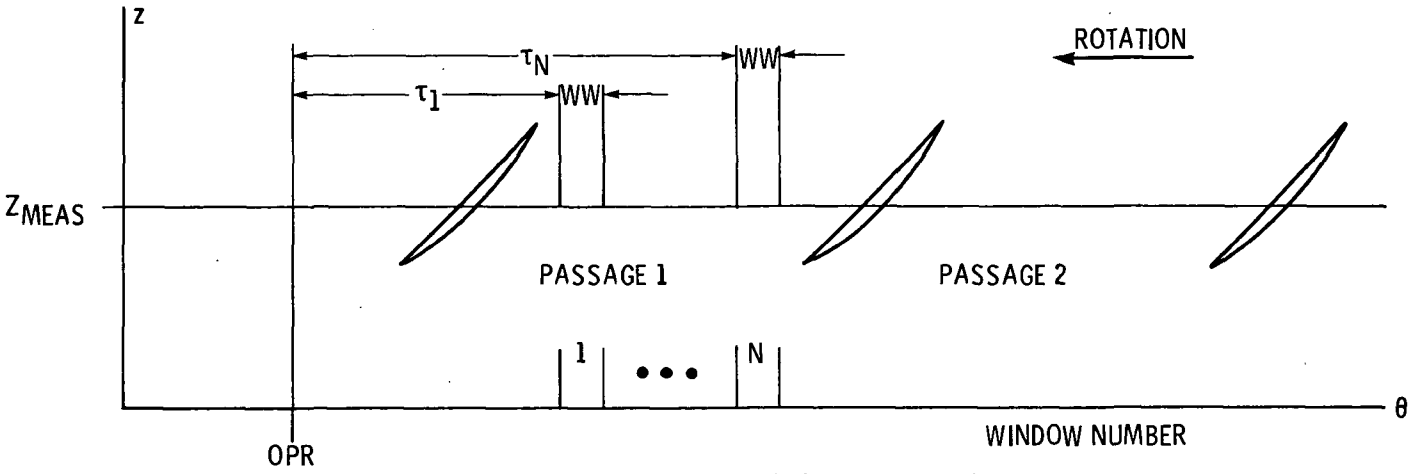

(a) Generation of one window per revolution.

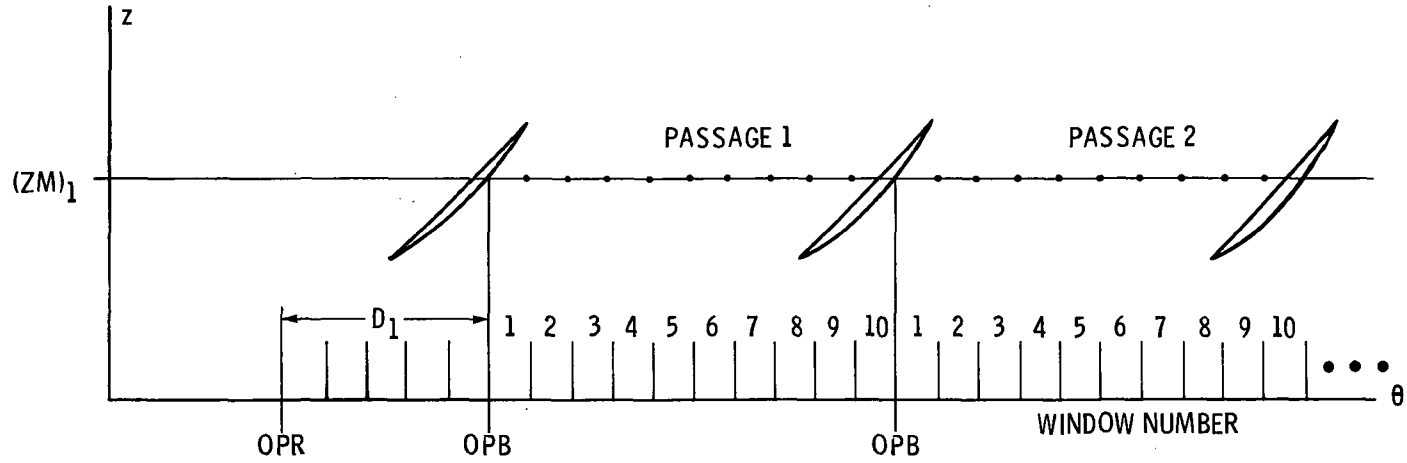

(b) Generation of windows once per blade passing.

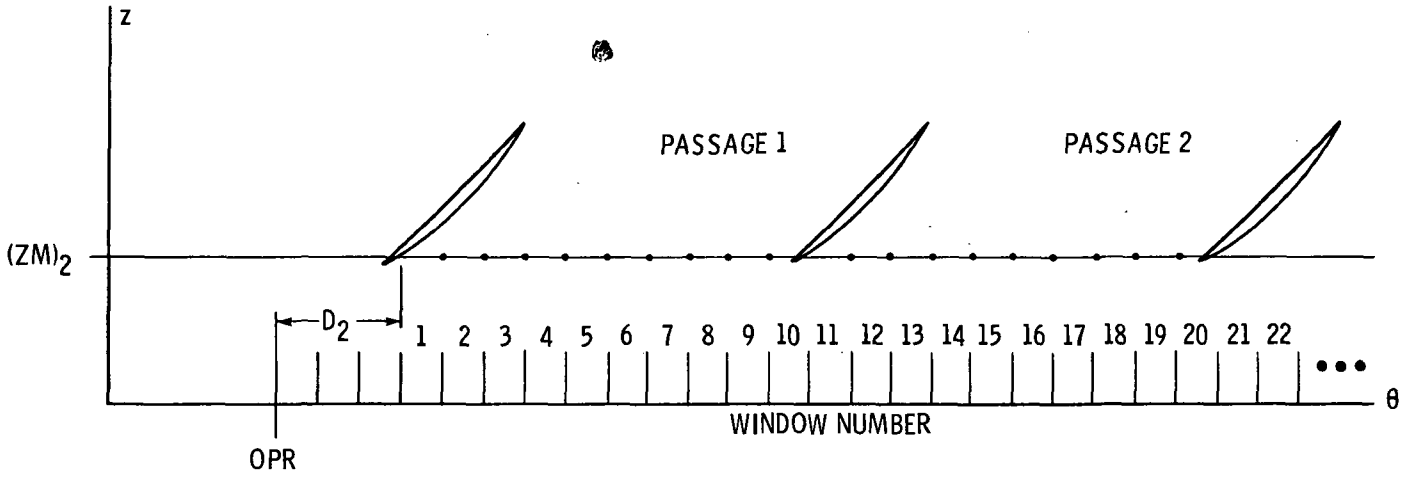

(c) Generation of continuous windows.

Figure 17. - Three methods of generating measurement windows for LA applications in rotating blade rows.

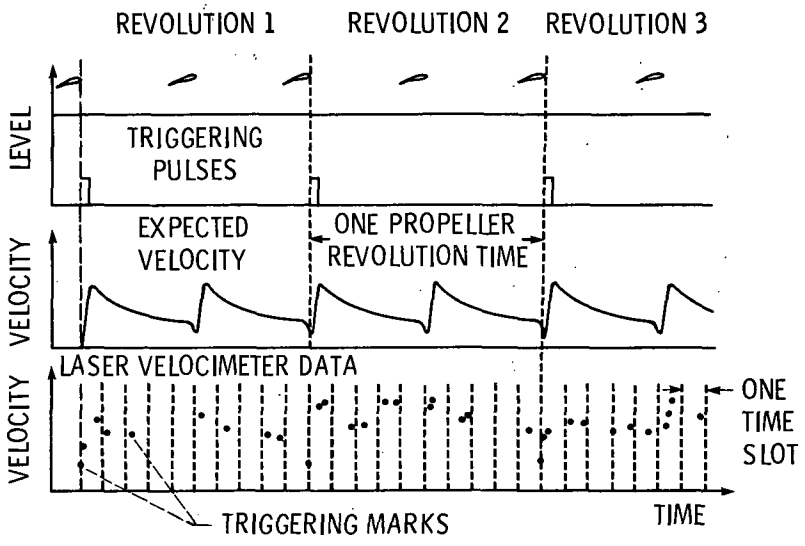

(a) Exact circumferential location of each measurement calculated using elapsed-time-between-measurements data and trigger pulse data.

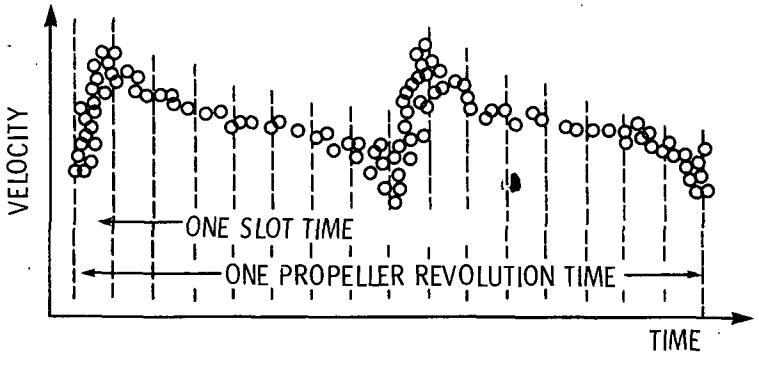

(b) Measurements assigned to proper window during post-run processing.

Figure 18. - Assignment of measurement windows during post-test data reduction.

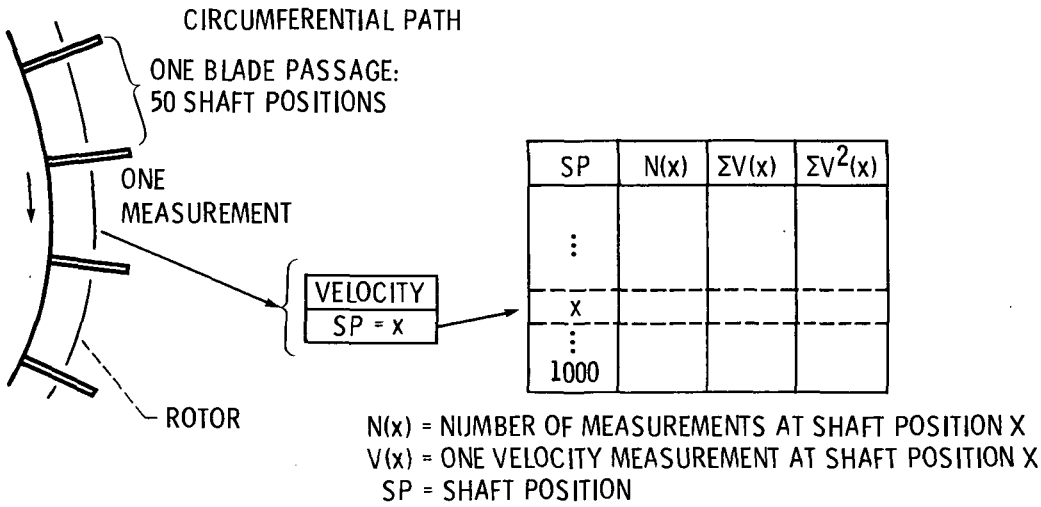

Figure 19. - Data storage scheme used during "window average" mode data acquisition.

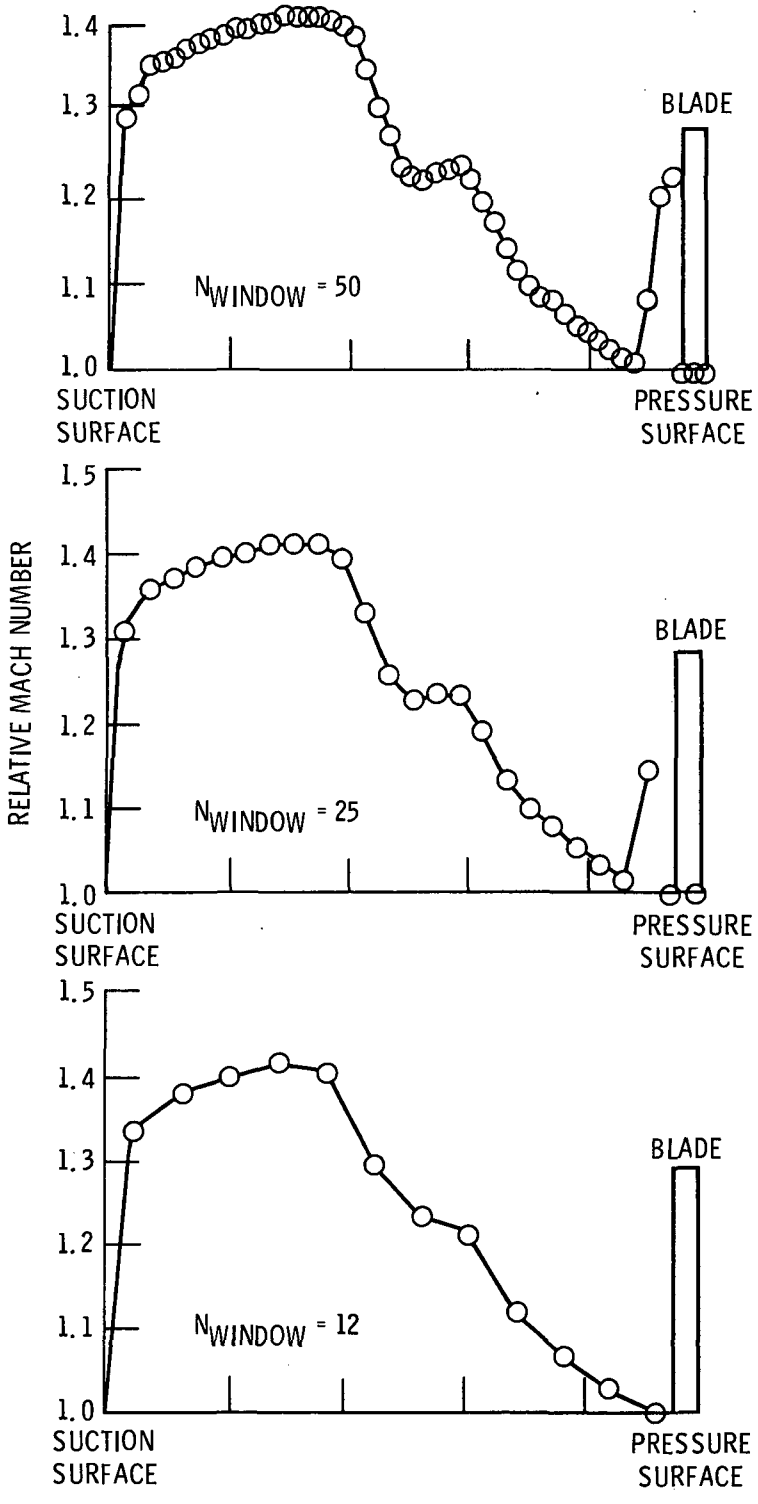

Figure 20. - Effect of window width on resolution of blade-to-blade velocity gradients.

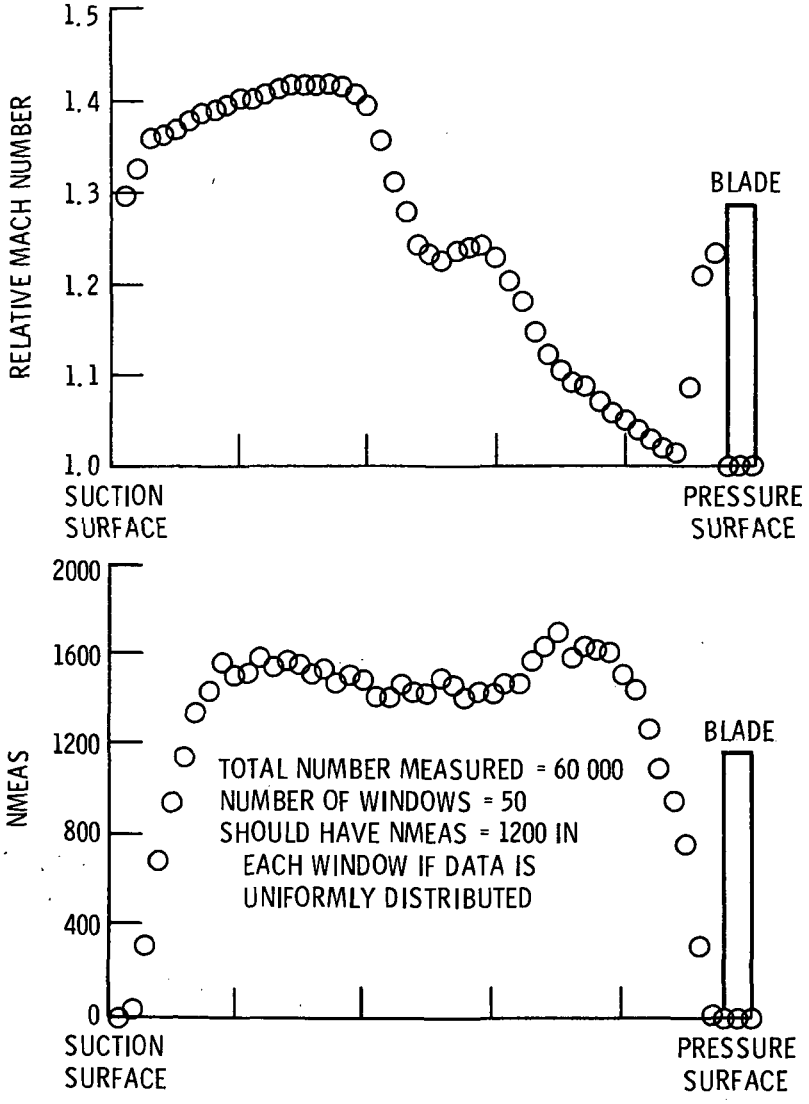

Figure 21. - Example of nonuniform distribution of the number of measurements which occur in each measurement window.

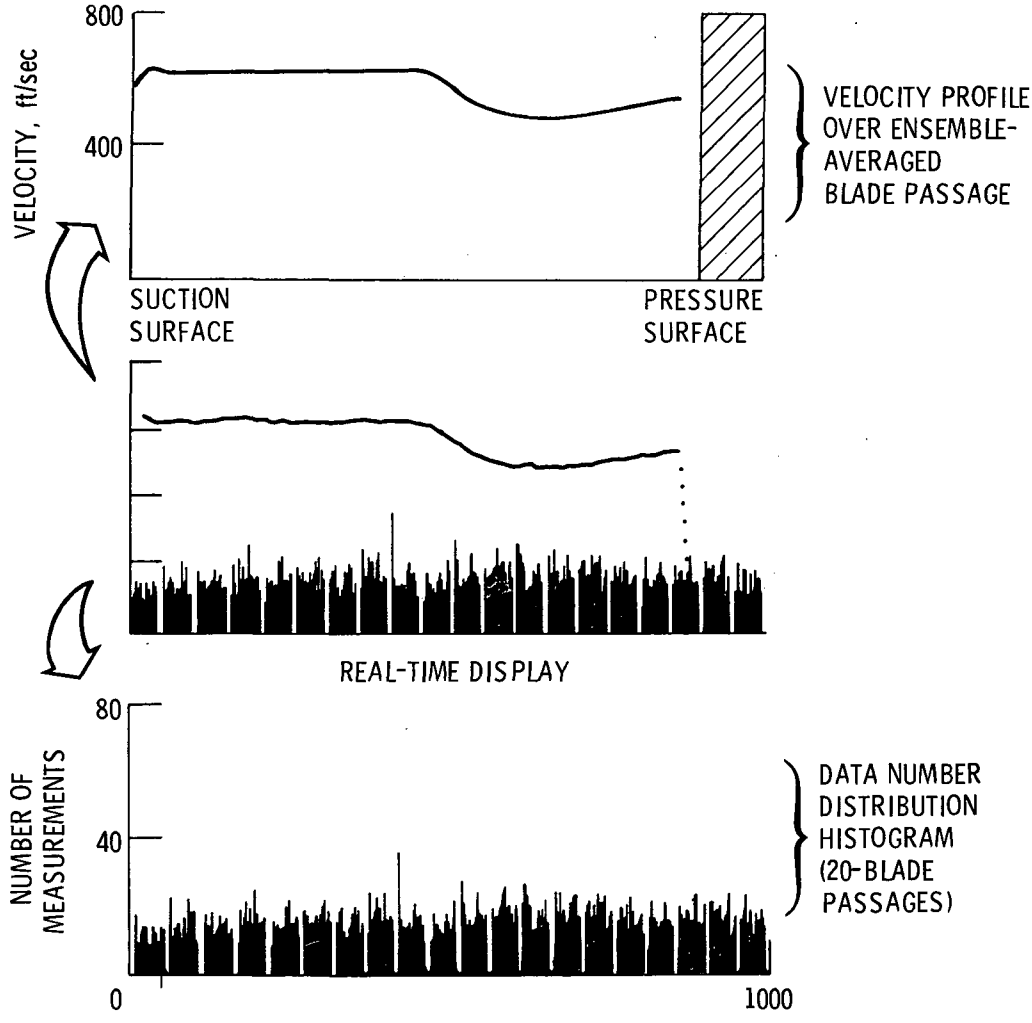

Figure 22. - Real-time display used in the NASA-Lewis LA system during compressor research testing.

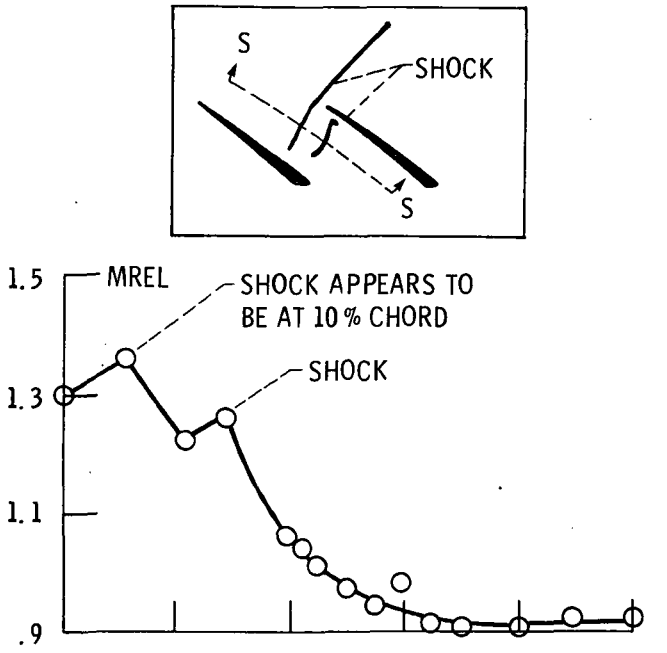

(a) Streamwise distribution (view S-S) of relative Mach number. Initial survey - every 10 % chord over first 40 % chord.

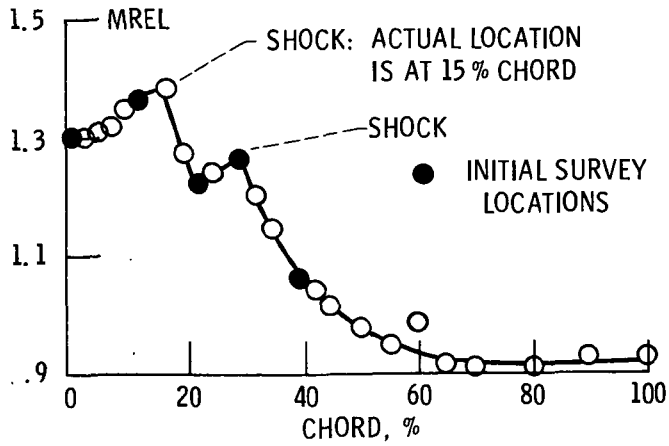

(b) Streamwise distribution (view S-S) of relative Mach number. Refinement of shock location using additional survey locations.

Figure 23. - Use of on-line data analysis to capture shock location in a transonic compressor.

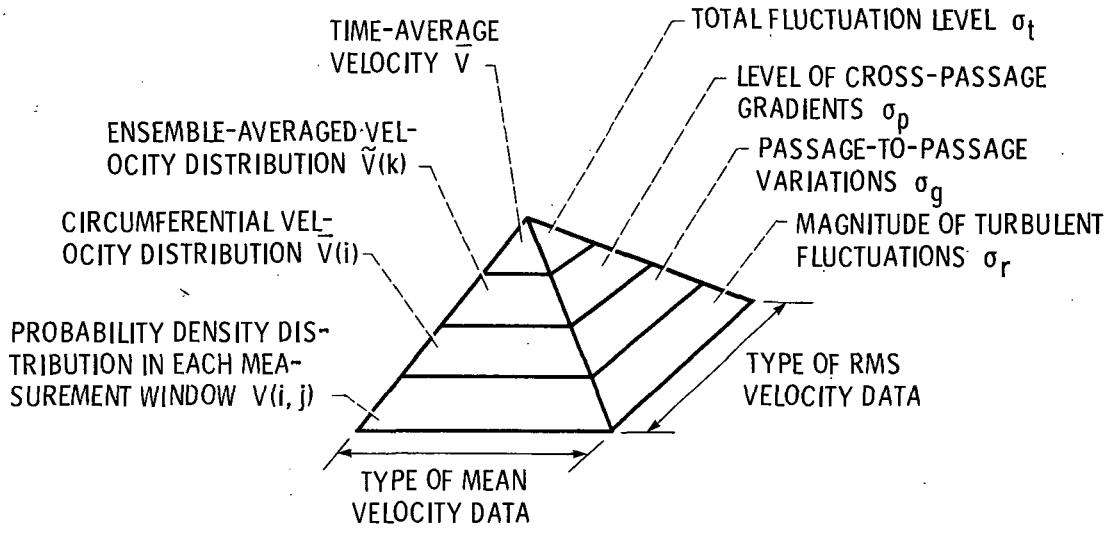

Figure 24. - Schematic representation of information available from LA data.

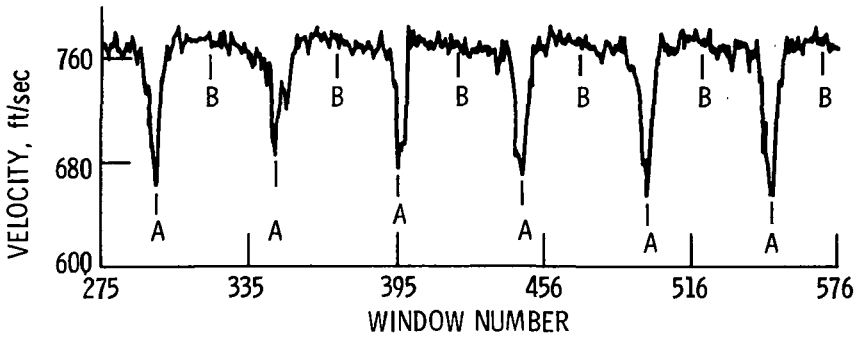

(a) Velocity distribution measured across 6 of the 17 measured blade passages.

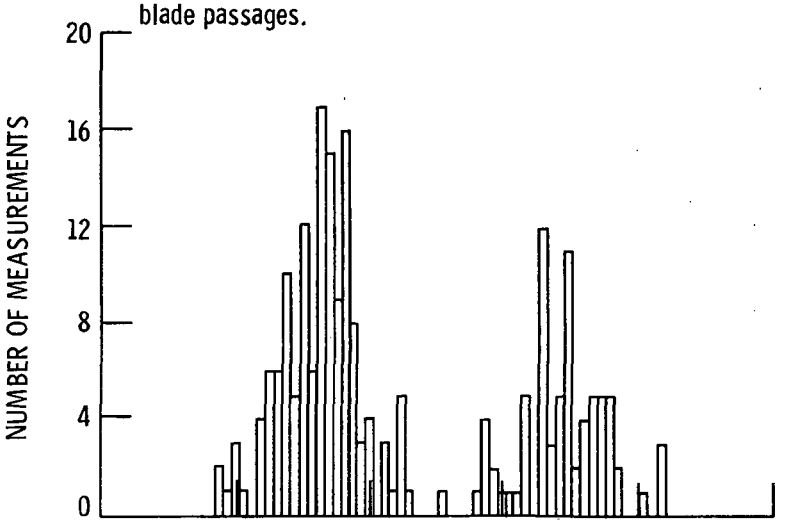

(b) p.d.d. for data acquired at point A in all 17 measured blade passages. Average velocity = 678.2.

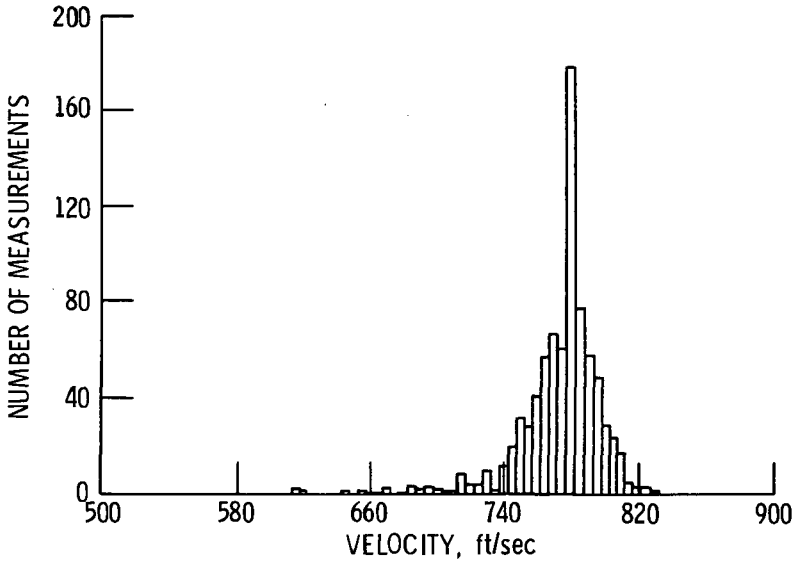

(c) p.d.d. for data acquired at point B in all 17 measured blade passages. Average velocity = 773.0.

Figure 25. - Blade-averaged probability density distributions.

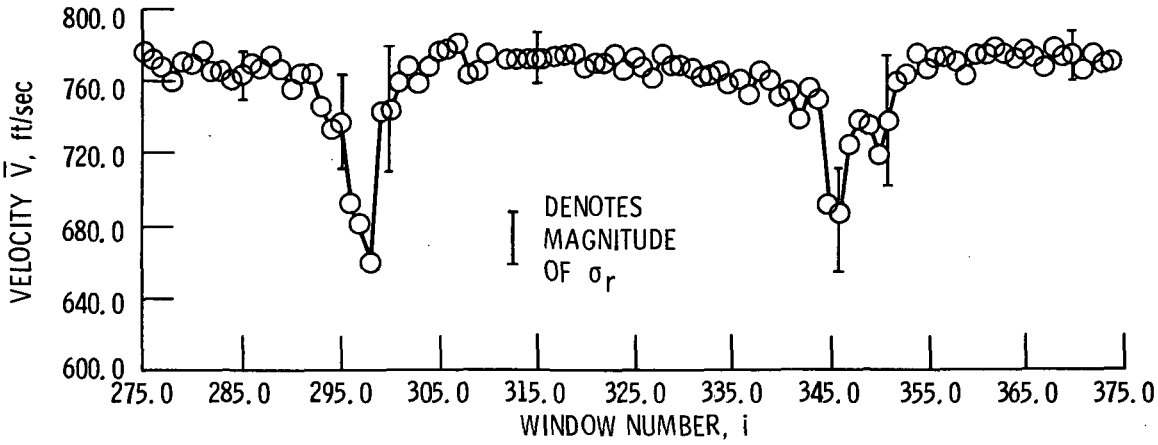

Figure 26. - Circumferential velocity distributions across two of the seventeen measured blade passages.

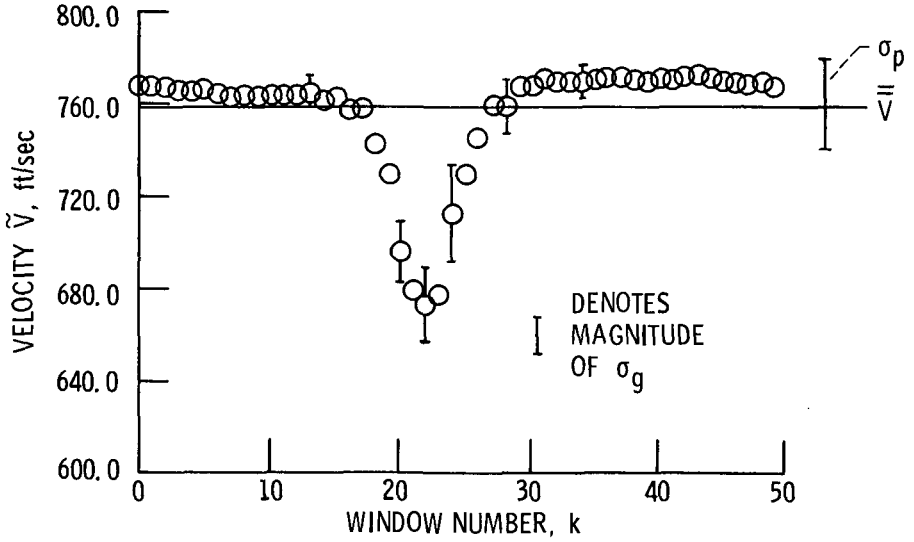

Figure 27. - Ensemble-averaged velocity distribution across the blade pitch.

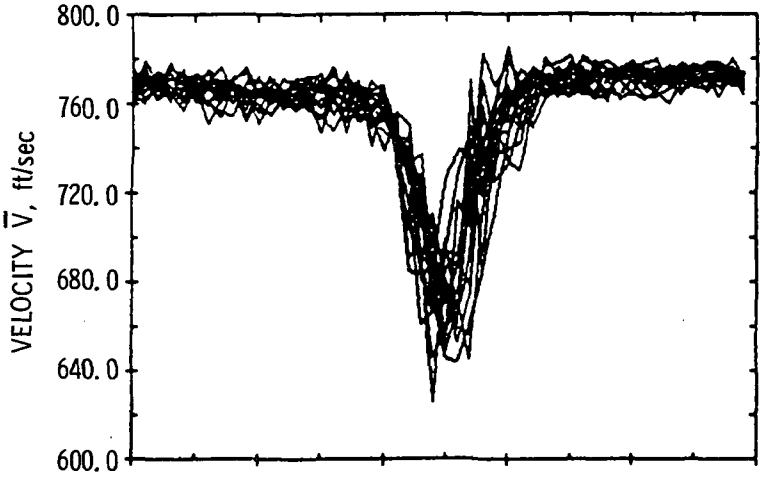

Figure 28. - Contribution of passage-to-passage flow variations to the total rms velocity level. Passage-to-passage flow field variations generate rms velocity σ_g.

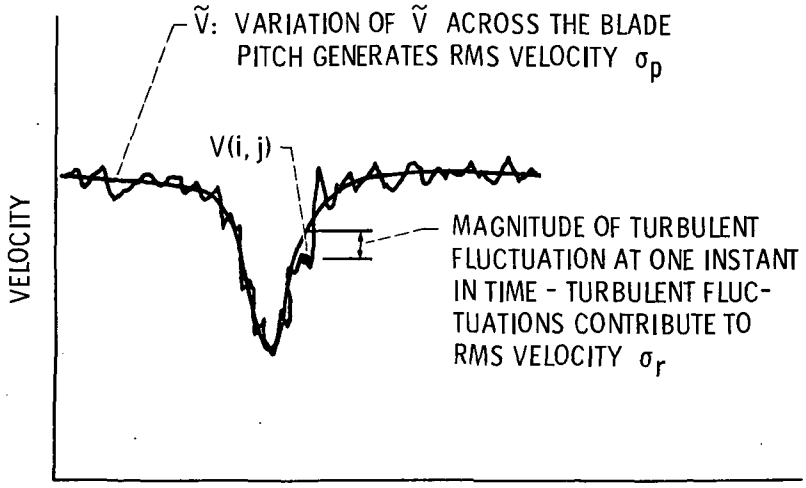

Figure 29. - Model used to illustrate various contributions to the total rms velocity level.

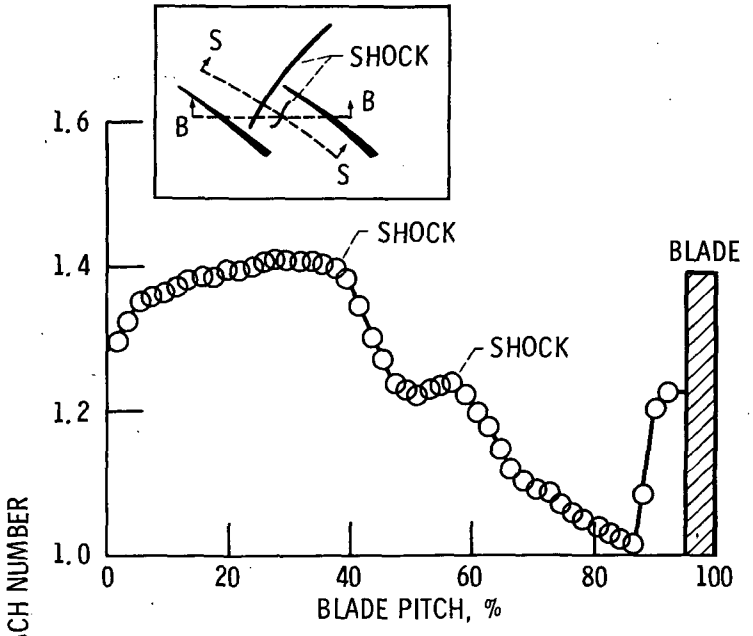

(a) Blade-to-blade distribution (view B-B) of relative Mach number.

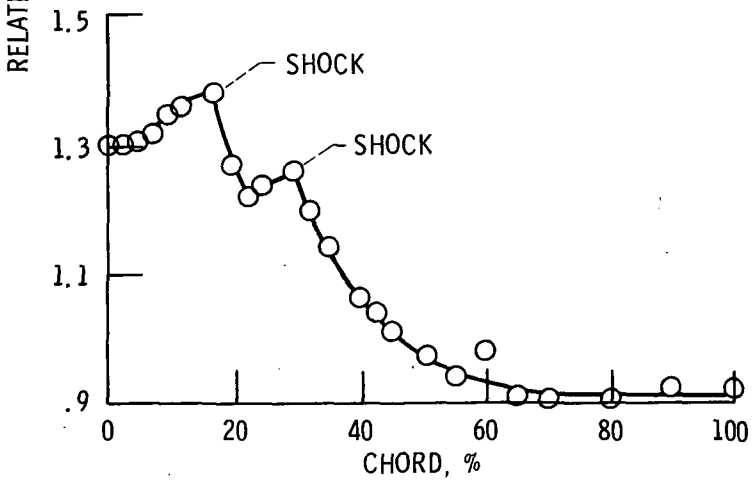

(b) Streamwise distribution (view S-S) of relative Mach number.

Figure 30. - Use of pitchwise and streamwise Mach number distributions to determine shock wave locations.

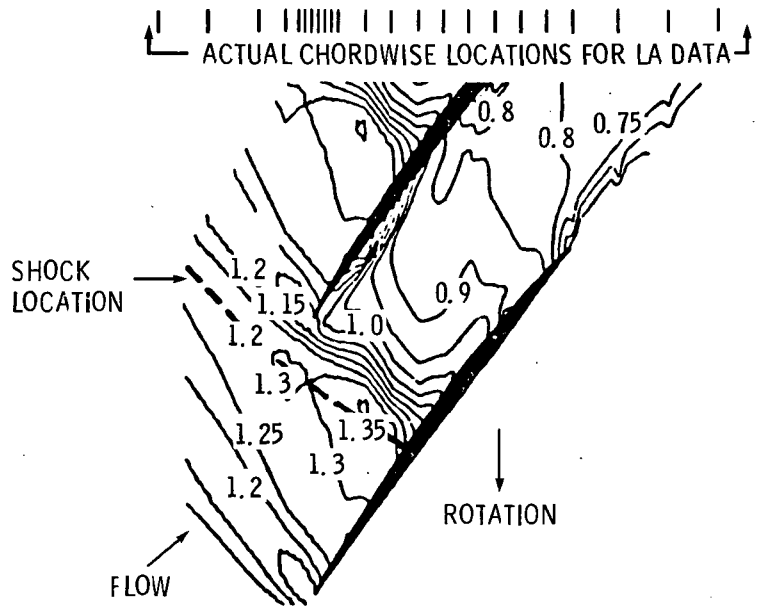

Figure 31. - Contour plot of relative Mach number distribution in a transonic fan.

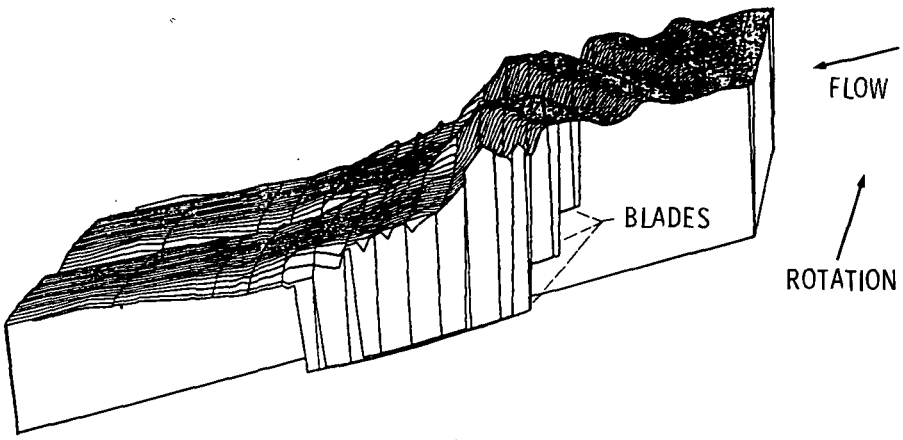

(a) Meridional view.

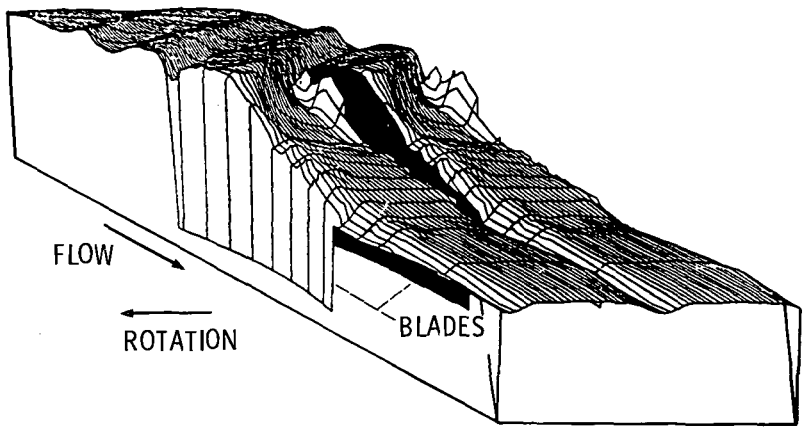

(b) View looking upstream.

Figure 32. - 3D hidden line plot of Mach number data from figure 31 viewed from two different directions.

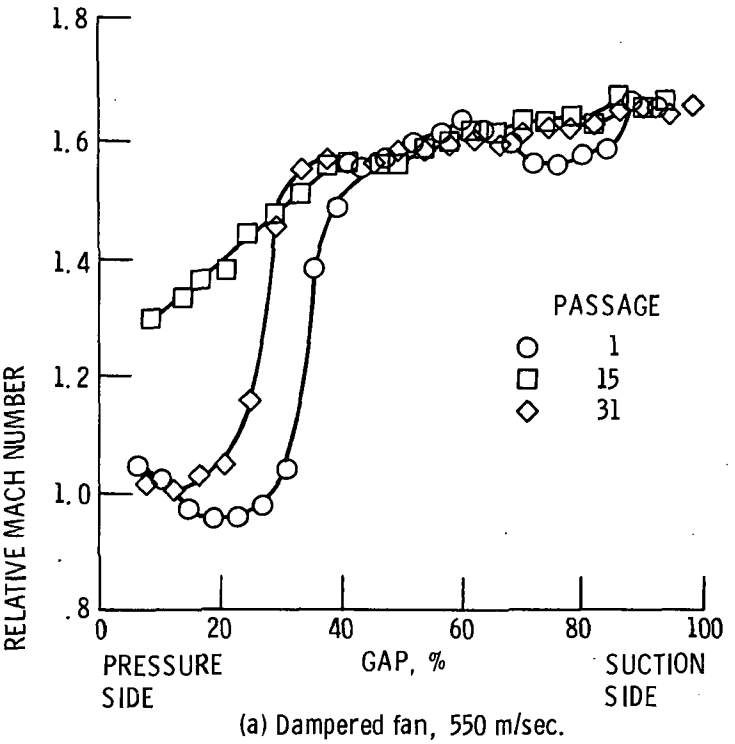

(a) Dampered fan, 550 m/sec.

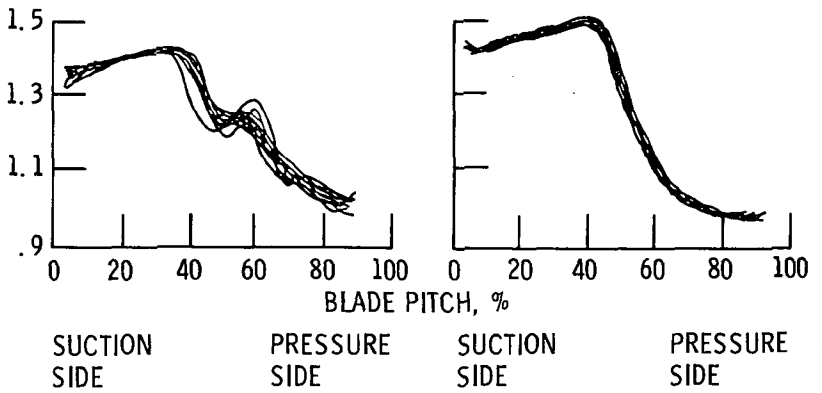

(b) Undampered fan, 429 m/sec.

Figure 33. - Passage-to-passage flow variations in two transonic axial flow fans.

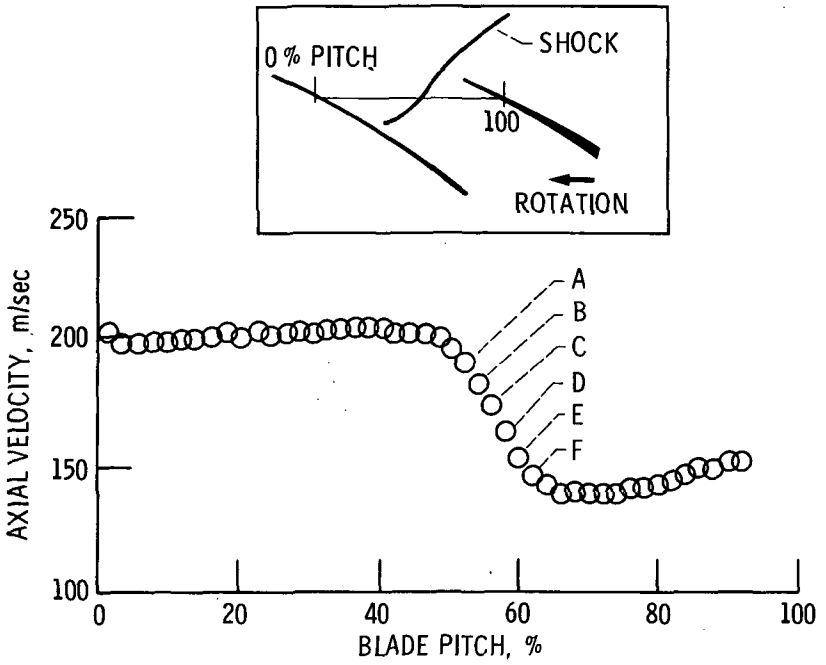

(a) Blade-to-blade distribution of mean axial velocity component.

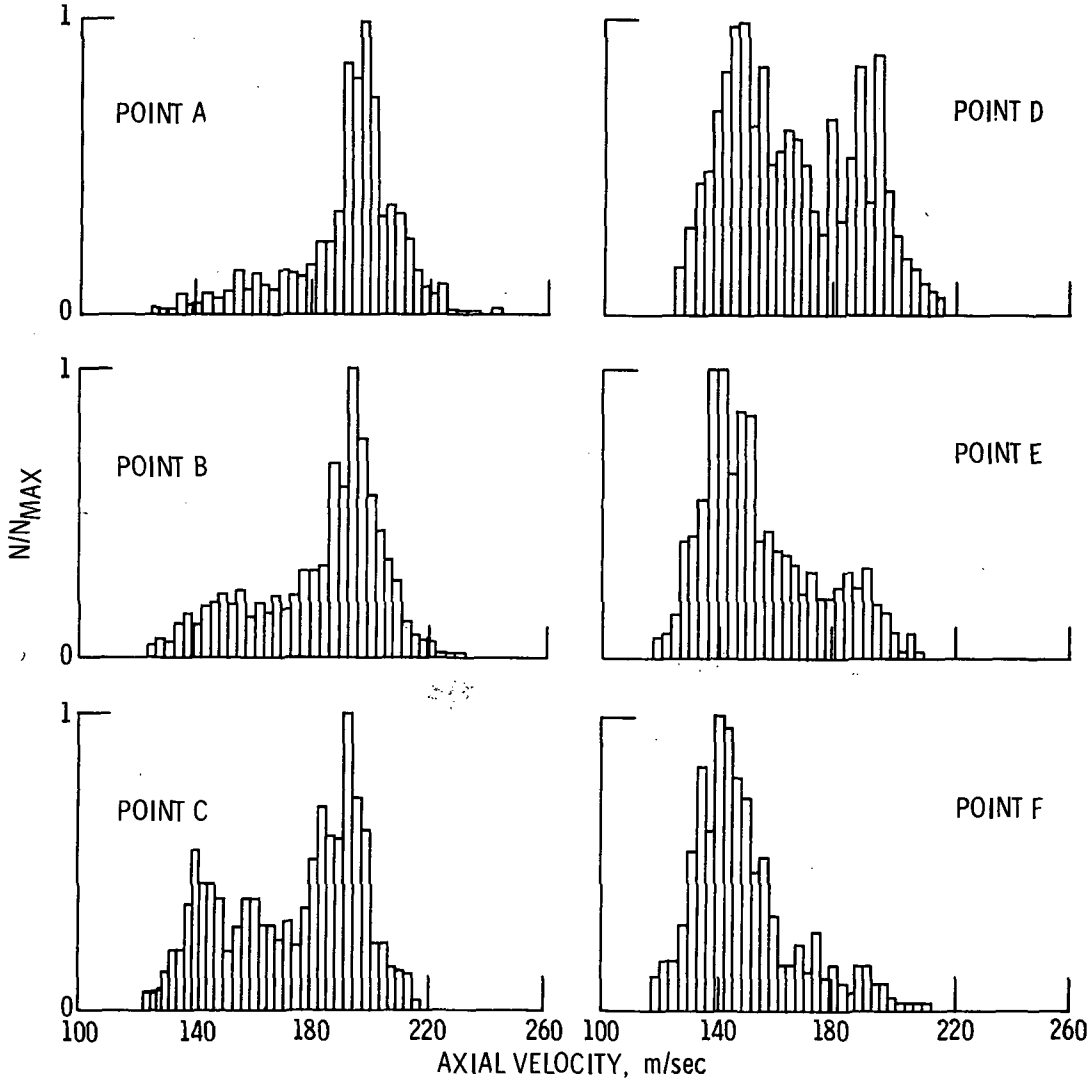

(b) Velocity probability at points near the passage shock.

Figure 34. - Analysis of rotor passage shock oscillations using velocity probability density distribution.

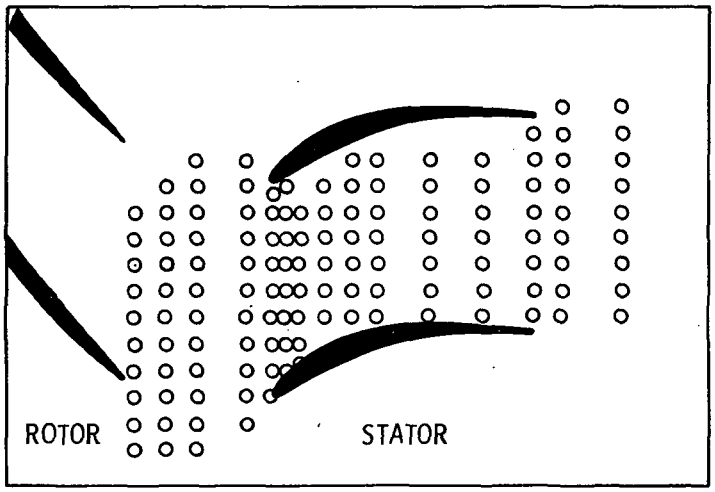

Figure 35. - LA survey locations used to investigate the periodically unsteady flow through a compressor stator.

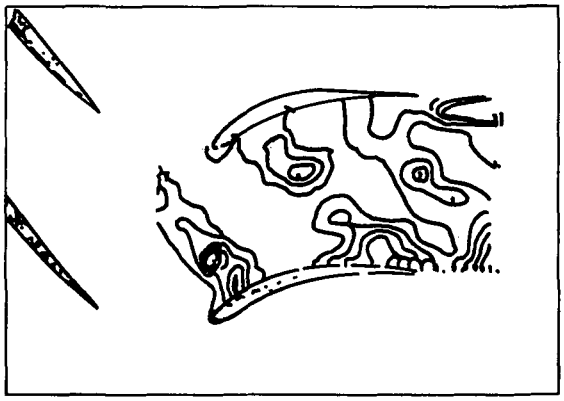

(a) Rotor trailing edge aligned circumferentially with stator leading edge.

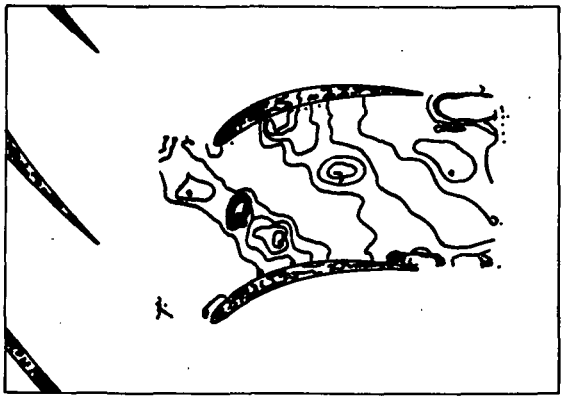

(b) Rotor displaced circumferentially by one-third rotor pitch.

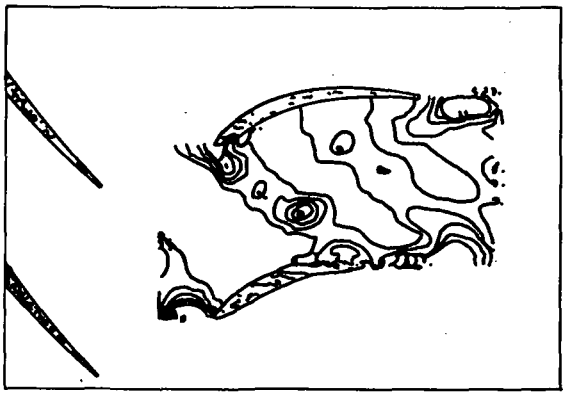

(c) Rotor displaced circumferentially by two-thirds rotor pitch.

Figure 36. - Periodically unsteady stator flow field at three points in the rotor-stator blade passing cycle. Distribution of turbulence intensity parallel to local temporary main flow direction (Tpar) within one stator blade passage.

1. Report No.	2. Government Accession No.	3. Recipient's Catalog No.
NASA TM-88798		

4. Title and Subtitle	5. Report Date
Laser Fringe Anemometry for Aero Engine Components	
	6. Performing Organization Code: 505-62-21

7. Author(s)	8. Performing Organization Report No.
Anthony J. Strazisar	E-3135
	10. Work Unit No.

9. Performing Organization Name and Address	11. Contract or Grant No.
National Aeronautics and Space Administration Lewis Research Center Cleveland, Ohio 44135	13. Type of Report and Period Covered: Technical Memorandum

12. Sponsoring Agency Name and Address	14. Sponsoring Agency Code
National Aeronautics and Space Administration Washington, D.C. 20546	

15. Supplementary Notes

Prepared for the 67th Symposium of the AGARD Propulsion and Energetics Panel on Advanced Instrumentation for Aero Engine Components, Philadelphia, Pennsylvania, May 19-23, 1986.

16. Abstract

Advances in flow measurement techniques in turbomachinery continue to be paced by the need to obtain detailed data for use in validating numerical predictions of the flowfield and for use in the development of empirical models for those flow features which cannot be readily modelled numerically. The use of laser anemometry in turbomachinery research has grown over the last 14 yr in response to these needs. Based on past applications and current developments, this paper reviews the key issues which are involved when considering the application of laser anemometry to the measurement of turbomachinery flowfields. Aspects of laser fringe anemometer optical design which are applicable to turbomachinery research are briefly reviewed. Application problems which are common to both laser fringe anemometry (LFA) and laser transit anemometry (LTA) such as seed particle injection, optical access to the flowfield, and measurement of rotor rotational position are covered. The efficiency of various data acquisition schemes is analyzed and issues related to data integrity and error estimation are addressed. Real-time data analysis techniques aimed at capturing flow physics in real time are discussed. Finally, data reduction and analysis techniques are discussed and illustrated using examples taken from several LFA turbomachinery applications.

17. Key Words (Suggested by Author(s))	18. Distribution Statement
Laser velocimeter Turbomachinery Instrumentation	Unclassified - unlimited STAR Category 02

19. Security Classif. (of this report)	20. Security Classif. (of this page)	21. No. of pages	22. Price*
Unclassified	Unclassified		

*For sale by the National Technical Information Service, Springfield, Virginia 22161